出國報告（出國類別：國際會議）

2016年歐洲地球科學聯盟年會出國報告

服務機關：國立暨南國際大學土木工程學系
姓名職稱：林俊廷　博士候選人
派赴國家：奧地利
出國期間：105年4月16日起至105年4月25日止
報告日期：105年6月20日

摘要

EGU(European Geosciences Union)是歐洲首屈一指的地球科學聯盟，共有來自全世界約 12500 的科學家所組成，舉辦大型研討會超過 20 年歷史，其年會為全球最大的地球科學盛會，致力於地質、海洋、大氣、天文等地球科學等相關議題進行論文發表與討論。

本次會議，係發表報告者近三年來的研究成果，論文名稱為：結合水準測量、航空照片與合成孔徑雷達等多時序資料進行深層滑動潛勢區繪製。本次以口頭英文發表，依照 EGU 投稿之子題約有一千餘篇論文，其中大約僅有 15~20%得以獲得口頭發表。

參與此次會議，除了進行研究發表之外，同時與國際學者交流，了解近年來雷達影像在山坡地監測的技術發展，以及各國的努力方向，在自然災害的監測議題上加以探討，得以與自身研究相輔相成，對日後研究方向能有所助益。

目次

參與此次會議目的

本次參加 2016 年歐洲地球科學聯盟年會係由『歐洲地球科學聯盟(The European Geosciences Union, EGU)』舉辦，該聯盟為 2002 年由『歐洲地球物理學會(the European Geophysical Society, EGS)』與『歐洲地球科學聯盟(the European Union of Geosciences, EUG)』兩學會合併而成。該學會致力於地質、海洋、大氣、天文等地球科學等相關議題發展與推動，為目前歐洲最大型的地球科學聯盟，亦與『美洲地球科學聯盟(American Geophysical Union, AGU)』為全球兩大地球科學研究團體。

本次年會共有 28 個子議題分類如下：

Special scientific events (SSE)	Geodynamics (GD)
Outreach, education, and media (OEM)	Geosciences Instrumentation & Data Systems (GI)
Short courses and topical meetings (STM)	Geomorphology (GM)
Feedback and networking (FAN)	Geochemistry, Mineralogy, Petrology & Volcanology (GMPV)
Administrative meetings (AM)	Hydrological Sciences (HS)
Interdisciplinary events (IE)	Natural Hazards (NH)
Atmospheric Sciences (AS)	Nonlinear Processes in Geosciences (NP)
Biogeosciences (BG)	Ocean Sciences (OS)
Climate: Past, Present, Future (CL)	Planetary & Solar System Sciences (PS)
Cryospheric Sciences (CR)	Seismology (SM)
Earth Magnetism & Rock Physics (EMRP)	Stratigraphy, Sedimentology & Palaeontology (SSP)

Energy, Resources and the Environment (ERE)	Soil System Sciences (SSS)
Earth & Space Science Informatics (ESSI)	Solar-Terrestrial Sciences (ST)
Geodesy (G)	Tectonics & Structural Geology (TS)

今年會議大約有 16000 多篇的文章發表，與去年相比增加約 2000 多篇，約有 13000 多人參與，而本次參加主要以自然災害(NaturalHazards)防災議題為首要項目，內容由氣象、山崩、火山、水文、地震海嘯、衛星遙測影像、地貌、地表災害管理至教育等領域所組成。

報告者研究內容屬於其中運用衛星遙測影像進行大規模地滑災害分析，差分干涉合成孔徑雷達影像(DInSAR)為主要應用之技術，該技術得以建置高精度的數值地形，同時可以監測出地表的微變量，本次與會者中，有相當多的研究者針對其技術應用提出新的應用面向及技術修正方向，除此之外無人載具、空拍影像、衛星光學影像、光達等遙測技術亦為近年來的發展方向，觀察並了解這類新技術的應用與研究成果，即為此次參與會議的主要目的。

出國過程及議程

本次會議期程從 105 年 4 月 17 日起至 105 年 4 月 22 日止，然奧地利與台灣之間約有 6 小時時差，故出發日為 4 月 16 日，回程班機考量到機票價差，故多滯留一日以節省經費支出，搭上 4 月 24 日班機返台，於 4 月 25 日清晨抵台，行程概要如下：

出差簡表

時間	地點	概要
4 月 16 日	桃園航空機場	機場報到與出發
4 月 17 日	維也納會場	報告
4 月 18 日	維也納會場	與會
4 月 20 日	維也納會場	口頭發表
4 月 21 日	維也納會場	與會
4 月 22 日	維也納會場	與會
4 月 23 日	維也納	滯留
4 月 24 日	維也納	機場報到與返航
4 月 25 日	桃園航空機場	抵達台灣

會議議程及聆聽簡報，製作為詳細時間表及對應題目，置於附件檔案中。

心得及建議

一、 MTInSAR 技術應用

InSAR 與 DInSAR（差分干涉合成孔徑雷達影像）等傳統方法雖可監測地表變形量達到釐米級的精度 ，但是僅限於資料條件良好的情況下。監測地表變形時時候以下因素會帶來誤差：去除地形影響時所用的 DEM 的誤差、大氣效應、軌道誤差、雜訊、解纏誤差等。小形變監測（<1cm/year ）會因為雷達波的強度不足，會被非形變的雜訊所覆蓋，而且通常要探測出小變形量需要較長時間，而長時間又會使干涉結果失去相關性。

MTInSAR（multi-temporal InSAR）是一種進階的差分干涉技術，其基礎原理是運用地表上的永久散射體（Persistent scatterer），萃取地面形變，減少失去相關性的問題，大致上有三種處理程序，第一種是干涉堆疊技術(PSInSAR)針對一幅主影像進行時間基線及空間基線的萃取，第二種為短基線分析法(SBASInSAR)，則是針對多幅影像進行基線篩選，第三種則是結合上述兩種方式進行分析。

透過 MTInSAR 分析的研究廣泛運用在這次會議中，因為它可以大幅降低大氣及軌道誤差，減少雜訊等優勢，使得研究結果更為可信，運用在台灣山區不無可行，但由於能得到良好地面訊息，須有充分的永久散射體於觀測區域，以台灣的山區遮蔽性而言，有一定的限制必須克服，所以另一個方式就是增加地面上的雷達回波強度，製作直角反射器當作永久散射體，在此次會議中也用與 GPS 進行比對，並得到良好的效果，可用於日後的研究參考。

二、 SENTINEL-1 衛星技術應用

（Sentinel-1）衛星是歐洲航天局哥白尼計劃（GMES）中的地球觀測衛星，由兩顆衛星組成，於參加會議時僅有第一顆已發射，並已開始進行觀測，於今年度將發射第二顆衛星，該衛星載有 C 波段合成孔徑雷達，可提

供連續圖像，一顆衛星可對同一地區以 12 天一次的週期進行觀測，當兩顆衛星都升空後，可提高為 6 天一次的週期。

C 波段的衛星波長較短，目前報告者的研究大多採用 L 波段的 ALOS 衛星，較短的波長雖可得到較高的解析度，但同時也會減少可觀測的地形變化量，一旦臨近網格超過半波長，就可能成為雜訊而失去相關性，由於與會者報告的案例，大多都為草原覆蓋的山丘，或是缺乏樹木的坡地區域，因此都能得到不錯的結果，若將之應用於台灣的地形條件，則還有許多問題需要克服。

哥白尼計畫同時也啟動了資源共享的機制，因此 Sentinel 衛星所產製的資料，可以透過網路下載取得，另一方面也將上述的 MTInSAR 分析方式建置於網站中，有興趣的研究者可透過線上分析，不用採購高昂的雷達影像處理軟體，就得到研究區域的干涉成果，但是使用條件也有所限制，可運用的參數不多，不能進行細膩的處理，在本次會議中並有開授 3 小時的操作課程，並可自行下載講義使用。

三、 建議

本次會議所獲得的資訊相當龐大，雷達影像技術在台灣目前的應用階段停留在容易觀測的平原區域，主要用於地層下陷、地震變形的探測，除了上述的近年來技術發展之外，同時也有其他運用處理過程的附屬產品，如同調性影像，進行沙丘變化量的探測等等，以及運用無人載具建模、分析地形變化、積雪深度等新式的遙測科技，報告者希冀能在充實國外研究與成果分享後，能將上述新技術調整及結合，運用於台灣山坡地監測，有助於日後災害潛勢的發展與應用。

	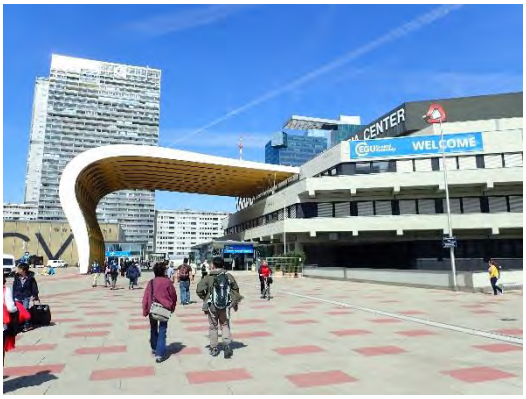
會場前長廊	會場大門
	
ＥＧＵ旗幟	海報、簡報上傳區
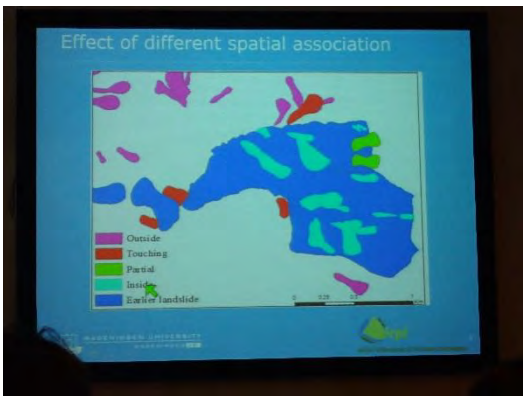	
簡報剪影	軟體操作教學剪影

附錄 1
會議行程表

Monday, 18 April

MO1, 08:30–10:00	**CR2.1**, Remote sensing of the cryosphere, **Orals**, **08:30–08:45**, **Room L2**
	GI3.2/EMRP4.18/ESSI1.7/NH8.6, Sensing techniques, geophysical methods, sensor network architectures and data analysis methods for critical and transport infrastructures monitoring and diagnostics (co-organized), **Orals**, **08:30–08:30**, **Room -2.31**
	NH2.3/GMPV7.4/SM7.7, The European contribution to the GEO Supersite initiative (co-organized), **Orals**, **08:30–08:45**, **Room L3** 09:15–09:30 EGU2016-13177 **A prototype of an automated high resolution InSAR volcano-monitoring system in the MED-SUV project** by **Tanvir A. Chowdhury**, Christian Minet, and Thomas Fritz
MO2, 10:30–12:00	**GI3.2/EMRP4.18/ESSI1.7/NH8.6**, Sensing techniques, geophysical methods, sensor network architectures and data analysis methods for critical and transport infrastructures monitoring and diagnostics (co-organized), **Orals**, **10:45–11:00**, **Room -2.31** 10:45–11:00 EGU2016-11231 **A Developed Spectral Identification Tree for Mineral Mapping using Hyperspectral Data** by **Fuping Gan**, Runsheng Wang, Bokun Yan, and Kun Shang 11:00–11:15 EGU2016-5293 **Quantitative extraction of bedrock exposed rate based on unmanned aerial vehicle data and TM image in Karst Environment** by **hongyan wang**, qiangzi li, xin du, and longcai zhao 11:15–11:30 EGU2016-7558 **Monitoring Ecological and Environmental Changes in Coastal Wetlands in the Yellow River Delta from 1987 to 2010 Using Remote Sensing Techniques** by **Kun Shang**, Dong Zhao, Fuping Gan, and Chenchao Xiao 11:30–11:45 EGU2016-17244 **Reconstruction of the sea surface elevation from the analysis of the data collected by a wave radar system** by **Giovanni Ludeno**, Francesco Soldovieri, Francesco Serafino, Claudio Lugni, Fabio Fucile, and Gabriele Bulian
	NH2.3/GMPV7.4/SM7.7, The European contribution to the GEO Supersite initiative (co-organized), **Orals**, **10:30–10:45**, **Room L3**
MO3, 13:30–15:00	**IE1.4/NP3.7/GI3.12/SSS9.32**, Multiscale modeling and analysis of environmental processes (co-organized), **Orals**, **13:30–13:30**, **Room 0.88** 13:45–14:00 EGU2016-14960 **Unsupervised DInSAR processing chain for multi-scale displacement analysis** by **Francesco Casu** and Michele Manunta 14:00–14:15 EGU2016-17225 **Modeling and analysis of Soil Erosion processes by the River Basins model: The Case Study of the Krivacki Potok Watershed, Montenegro** by **Dusko Vujacic**, Goran Barovic, Dragica Mijanovic, Velibor Spalevic, Milic Curovic, Vjekoslav Tanaskovic, and Nevenka Djurovic 14:15–14:30 EGU2016-6893 **Ballistic analysis during multiscale explosive eruption at Vesuvius and hazard implications** by **Vincenzo De Novellis** 14:30–14:45 EGU2016-9147 **Magnetotellurics as a multiscale geophysical exploration method** by **Rolando Carbonari**, Luca D'Auria, Rosa Di Maio, and Zaccaria Petrillo
	NH2.3/GMPV7.4/SM7.7, The European contribution to the GEO Supersite initiative (co-organized), **Orals**, **13:30–13:45**, **Room L3**
MO4, 15:30–17:00	**NH3.6**, Prediction and forecasting of landslides, **Orals**, **15:30–15:45**, **Room L3** 15:30–15:45 EGU2016-1767 **A framework for nowcasting and forecasting of rainfall-triggered landslide activity using remotely sensed data** by **Dalia Kirschbaum** and Thomas Stanley 15:45–16:00 EGU2016-408 **Utilization of web-based stationary rainfall data for near-real-time derivation of spatial landslide susceptibility** by **Ekrem Canli**, Thomas Glade, and Bernd Loigge

	16:00–16:15 EGU2016-1304 **What rainfall events trigger landslides on the West Coast US?** by **Michela Biasutti**, Richard Seager, and Dalia Kirschbaum 16:15–16:30 EGU2016-15006 **Satellite-rainfall estimation for identification of rainfall thresholds used for landslide/debris flow prediction** by Viviana Maggioni, **Efthymios I. Nikolopoulos**, Francesco Marra, Elisa Destro, and Marco Borga 16:30–16:45 EGU2016-125 **Do landslides follow landslides?** by **Jalal Samia**, Arnaud Temme, Arnold Bregt, Jakob Wallinga, Fausto Guzzetti, Francesca Ardizzone, and Mauro Rossi 16:45–17:00 EGU2016-16411 **Landslide response signatures from storm Desmond (UK)/Synne (Norway), December 2015.** by **Tom Dijkstra**, Katy Freeborough, Helen Reeves, Boje Soren Nykjaer, Monica Sund, Graziella Devoli, and Vanessa Banks
MO5, 17:30–19:00	**NH3.6**, Prediction and forecasting of landslides, **Orals**, **17:45–18:00**, **Room L3** 17:30–17:45 EGU2016-14820 **Geomorphological characteristics of increased landslide activity in the Gudbrandsdalen valley, Norway** by **Håkon Heyerdahl** and Øyvind Høydal 17:45–18:00 EGU2016-17793 **Calibration of back-analysed model parameters for landslides using classification statistics** by **Jose Cepeda** and Laura Henderson 18:00–18:15 EGU2016-10543 **Andic soil features and debris ?ows in Italy. New perspective towards prediction** by **Solange Scognamiglio**, Domenico Calcaterra, Michela Iamarino, Giuliano Langella, Nadia Orefice, Simona Vingiani, and Fabio Terribile 18:15–18:30 EGU2016-14471 **A Novel Approach based on GPS/GNSS Surveying to Monitor Excessive Active Landslide: A Case Study of Intepe Landslide** by **Deniz Güngördü**, R Cuneyt Ereno?lu, Özgün Akcay, and Oya Ereno?lu 18:30–18:45 EGU2016-10988 **GIS based probabilistic analysis for shallow landslide susceptibility using Point Estimate Method** by **Hyuck-Jin Park** and Jung-Hyun Lee 18:45–19:00 EGU2016-2234 **A study of landslide warning based on the RTI model in Korea** by **Byung-Gon Chae**, Ko-Fei Liu, and Junghae Choi
MO5, 17:30–19:00	**IE1.4/NP3.7/GI3.12/SSS9.32**, Multiscale modeling and analysis of environmental processes (co-organized), **Posters**, **08:00–19:30**, **Hall X4** X4.272 EGU2016-14226 **Time Series Analysis OF SAR Image Fractal Maps: The Somma-Vesuvio Volcanic Complex Case Study** by **Antonio Pepe**, Claudio De Luca, Gerardo Di Martino, Antonio Iodice, Mariarosaria Manzo, Susi Pepe, Daniele Riccio, Giuseppe Ruello, Eugenio Sansosti, and Ivana Zinno
	CR2.1, Remote sensing of the cryosphere, **Posters**, **08:00–19:30**, **Hall X4** X4.142 EGU2016-6408 **Outlet-glacier flow dynamics estimation combining in-situ and spaceborne SAR measurements** by **Christoph Rohner**, Daniel Henke, David Small, Rémy Mercenier, Martin Lüthi, and Andreas Vieli
	NH2.3/GMPV7.4/SM7.7, The European contribution to the GEO Supersite initiative (co-organized), **Posters**, **08:00–19:30**, **Hall D**
	NH3.6, Prediction and forecasting of landslides, **Posters**, **08:00–19:30**, **Hall D** D.187 EGU2016-381 **Hydro-meteorological analysis of slope failures occurred in 2014 in the Ialomita Subcarpathians, Romania** by **Zenaida Chitu**, Thom Bogaard, Aristita Busuioc, Sorin Burcea, Ionut Sandric, and Mary-Jeanne Adler D.188 EGU2016-963 **Structural control of landslides. A regional approach based on a developed ArcGIS tool** by **Viorel Ilinca**, Ionu? ?andric, Zenaida Chi?u, and Marta Jurchescu

D.189 EGU2016-1184 **Rainfall Threshold of Triggering Landslide-an Example of Typhoon Soudelor in 2015** by **Yong-Jun Lin**, Ji-Hua Lin, and Yih-Chi Tan

D.190 EGU2016-2229 **A landslide susceptibility prediction on a sample slope in Kathmandu Nepal associated with the 2015's Gorkha Earthquake** by **Tetsuya Kubota** and Prem Prasad Paudel

D.191 EGU2016-2451 **Simulation of Sediment Transport Caused by Landslide at Nanhua Reservoir Watershed in Southern Taiwan** by **Ming-Hsi Lee**, Cong-Gi Huang, and Huan-Hsuan Lin

D.192 EGU2016-2482 **An establishment on the hazard mitigation system of large scale landslides for Zengwen reservoir watershed management in Taiwan** by **Kuang-Jung Tsai**, Ming-Hsi Lee, Yie-Ruey Chen, Meng-Hsuan Huang, and Chia-Ching Yu

D.193 EGU2016-2491 **Development and application of a modified wireless tracer for disaster prevention** by **Han Chung Yang** and Chih Chiang Su

D.194 EGU2016-2532 **Assessment of Rainfall-induced Landslide Potential and Spatial Distribution** by **Yie-Ruey Chen**, Kuang-Jung Tsai, Jing-Wen Chen, Jie-Lun Chiang, Shun-Chieh Hsieh, and Yung-Sheng Chue

D.195 EGU2016-3379 **A zonation technique for landslide susceptibility in southern Taiwan** by **Jie-Lun Chiang**, Yu-Qing Tian, Yie-Ruey Chen, and Kuang-Jung Tsai

D.196 EGU2016-3672 **A hybrid hydrologically complemented warning model for shallow landslides induced by extreme rainfall in Korean Mountain** by **Ananta Man Singh Pradhan**, Hyo-Sub Kang, and Yun-Tae Kim

D.197 EGU2016-4480 **Characterising regional landslide initiation thresholds in Scotland, UK using NIMROD c-band precipitation radar and the BGS National Landslide Database.** by **Benjamin Postance**, John Hillier, Tom Dijkstra, and Neil Dixon

D.198 EGU2016-4496 **Comparison and applicability of landslide susceptibility models based on landslide ratio-based logistic regression, frequency ratio, weight of evidence, and instability index methods in an extreme rainfall event** by **Chunhung Wu**

D.199 EGU2016-5552 **Characteristics and rainfall threshold of deep-seated landslide in Taiwan** by **Lun-Wei Wei** and Hongey Chen

D.200 EGU2016-5693 **Preliminary Geotechnical Investigation of Two Basaltic Landslide Sites in Mauritius, Offshore Africa** by **Bhoopendra Dabycharun**, Takeshi Kuwano, Kensuke Ichikawa, and Hiroshi Fukuoka

D.201 EGU2016-5704 **Delineation of potential deep seated landslides in a watershed using environmental index** by **Siao Ying Lai**, Chao Yuan Lin, and Cheng Yu Lin

D.202 EGU2016-5787 **The Rainfall and Rainfall Kinetic Energy Intensity-Duration of Landslides and Debris flow in Taiwan** by **Jui-Ming Chang** and Hongey Chen

D.203 EGU2016-5923 **An integrated mass wasting susceptibility assesment by geographical information systems and remote sensing applications: Example from North Turkey** by **Aykut Akgün**

D.204 EGU2016-5954 **Combined statistical analysis of landslide release and propagation** by **Martin Mergili**, Mohammad Rohmaneo, and Hone-Jay Chu

D.205 EGU2016-7715 **Shallow landslide susceptibility model for the Oria river basin, Gipuzkoa province (North of Spain). Application of the logistic regression and comparison with previous studies.** by **Txomin Bornaetxea**, Iñaki Antigüedad, and Orbange Ormaetxea

D.206 EGU2016-7779 **Estimation of debris-flow prone basins based on geomorphic quantities and rainfall amount on granite slopes in Japan** by **Tsuyoshi Wakatsuki**, Masato Sato, Yasuhiro Inomata, Naofumi Takeda, and Shinya Aoki

D.207 EGU2016-8620 **Wi-GIM system: a new wireless sensor network (WSN) for accurate ground instability monitoring** by **Lorenzo Mucchi**, Federico Trippi, Rosa Schina, Alessandro Fornaciai, Giovanni Gigli, Luca Nannipieri, Massimiliano Favalli, Jordi Marturia Alavedra, Emanuele Intrieri, Andrea Agostini, Ennio Carnevale, Giovanni Bertolini, Marco Pizziolo, and Nicola Casagli

D.208 EGU2016-10931 **Improving the early-warning of a mud-debris flow using radar rainfall data** by **Hwandon Jun**, Soojun Kim, and Jiho Lee

D.209 EGU2016-14092 **An integrated analysis of surface velocities induced by rainfall in the Séchilienne landslide (Western Alps, France)** by Clara Lévy, **Séverine Bernardie**, Marie-Aurélie Chanut, Antonio Abellan-Fernandez, Aurélien Vallet, Laurent Dubois, Michel Jaboyedoff, and Catherine Bertrand

D.210 EGU2016-15089 **Soil moisture in relation to landslide triggering in Asturias (NW Spain)** by **Pablo Valenzuela**, María José Domínguez-Cuesta, Manuel Antonio Mora García, and Montserrat Jiménez-Sánchez

D.211 EGU2016-17361 **Slopeland utilizable limitation classification using landslide inventory** by **Shu Fen Tsai** and Chao Yuan Lin

D.212 EGU2016-17676 **The relationship among probability of failure, landslide susceptibility and rainfall** by **Chuen Ming Huang** and Chyi-Tyi Lee

Tuesday, 19 April

TU1, 08:30–10:00	**NH9.1**, Natural hazard event analyses for risk reduction and adaptation, **Orals**, **08:30–08:30**, **Room N2** 08:30–08:45 EGU2016-2208 **From event analysis to global lessons: disaster forensics for building resilience** by **Adriana Keating**, Kanmani Venkateswaran, Michael Szoenyi, Karen MacClune, and Reinhard Mechler 08:45–09:00 EGU2016-1357 **Are we overestimating the effect of large-scale indices of climate variability in floods and droughts in Europe?** by **Gabriela Guimarães Nobre**, Jeroen Aerts, and Philip J. Ward 09:15–09:30 EGU2016-6503 **Rebuilt risk: involuntary return, voluntary migration, and socioeconomic segregation in post-tsunami Aceh** by **Jamie McCaughey**, Patrick Daly, Ibnu Mundzir, Saiful Mahdi, and Anthony Patt 09:30–09:45 EGU2016-7609 **Assessment of crop damage and hail risk based on radar hail signature information** by **Satyanarayana Tani**, Helmut Paulitsch, Reinhard Teschl, and Barbara Süsser-Rechberger
TU2, 10:30–12:00	**NH9.1**, Natural hazard event analyses for risk reduction and adaptation, **Orals**, **10:30–10:30**, **Room N2** 11:30–11:45 EGU2016-17160 **Vulnerability of electricity transmission infrastructure to natural hazards** by **Nadejda Komendantova**
	NP4.5/ESSI1.5, Big data and machine learning in geosciences (co-organized), **Orals**, **11:00–11:15**, **Room -2.16** 11:45–12:00 EGU2016-16445 **Land cover in the Guayas Basin using SAR images from low resolution ASAR Global mode to high resolution Sentinel-1 images** by **Luc Bourrel**, Nicolas Brodu, and Frédéric Frappart
TU3, 13:30–15:00	**GI2.5**, Sentinel 1 for Science, INSAR results, **Orals**, **13:30–13:45**, **Room L3** 13:30–13:45 EGU2016-13316 **The 2015 Gorkha earthquake investigated from radar satellites: slip and stress modeling along the MHT** by **Faqi Diao**, Thomas R. Walter, Mahdi Motagh, Pau Prats, Rongjiang Wang, and Sergey Samsonov 13:45–14:00 EGU2016-9763 **3D displacement field of the 2015 Mw8.3 Illapel earthquake (Chile) from across- and along-track Sentinel-1 TOPS interferometry** by **Raphaël Grandin** 14:00–14:15 EGU2016-15136 **Sentinel-1 DInSAR processing chain within Geohazard Exploitation Platform** by **Ivana Zinno**, Manuela Bonano, Sabatino Buonanno, Francesco Casu, Claudio De Luca, Adele Fusco, Riccardo Lanari, Michele Manunta, Mariarosaria Manzo, Chandrakanta Ojha, and Antonio Pepe 14:15–14:30 EGU2016-16037 **Sentinel-1 Constellation for nationwide deformation mapping with InSAR -- From science to operations** by **John Dehls**, Yngvar Larsen, and Petar Marinkovic 14:30–14:45 EGU2016-14756 **Sentinel-1 automatic processing chain for volcanic and seismic areas monitoring within the Geohazards Exploitation Platform (GEP)** by **Claudio De Luca**, Ivana Zinno, Michele Manunta, Riccardo Lanari, and Francesco Casu 14:45–15:00 EGU2016-2920 **Persistent Scatterer Interferometry using Sentinel-1 Data** by **Oriol Monserrat**, Michele Crosetto, Nuria Devanthery, Maria Cuevas-Gonzalez, Huang Qihuan, Anna Barra, and Bruno Crippa
	NP4.5/ESSI1.5, Big data and machine learning in geosciences (co-organized), **Orals**, **13:30–13:45**, **Room -2.16**
	SM2.1/NH4.10, Imaging and Modeling of Earthquake Sources (co-organized), **Orals**, **13:30–13:30**, **Room K2**

TU4, 15:30–17:00	**SM2.1/NH4.10**, Imaging and Modeling of Earthquake Sources (co-organized), **Orals**, **16:15–16:30**, **Room K2**
TU5, 17:30–19:00	**GI3.2/EMRP4.18/ESSI1.7/NH8.6**, Sensing techniques, geophysical methods, sensor network architectures and data analysis methods for critical and transport infrastructures monitoring and diagnostics (co-organized), **Posters**, **08:00–19:30**, **Hall A**
	NH9.1, Natural hazard event analyses for risk reduction and adaptation, **Posters**, **08:00–19:30**, **Hall D**
	NP4.5/ESSI1.5, Big data and machine learning in geosciences (co-organized), **Posters**, **08:00–19:30**, **Hall A**
	SM2.1/NH4.10, Imaging and Modeling of Earthquake Sources (co-organized), **Posters**, **08:00–19:30**, **Hall X2** X2.18 EGU2016-16000 **Kinematic source parameter estimation for the 1995 Mw 7.2 Gulf of Aqaba Earthquake by using InSAR and teleseismic data in a Bayesian framework** by **Hannes Bathke**, Guangcai Feng, Sebastian Heimann, Mehdi Nikkhoo, Olaf Zielke, Sigurjon Jónsson, and Martin Mai

Wednesday, 20 April

WE1, 08:30–10:00

NH3.3/SSS12.28, Characterizing and monitoring landslide processes using remote sensing and geophysics (co-organized), **Orals**, **08:30–08:30**, **Room N2**

08:30–08:45 EGU2016-16117 **Dynamics of the Askja caldera landslide, July 2014, from seismic signal analysis** by **Anne Schöpa**, Arnaud Burtin, Niels Hovius, and Robert G. Green

08:45–09:00 EGU2016-17866 **An insight into the mechanics of rockfalls using observations and modelling: a case study in the Dolomieu crater of Piton de la Fournaise, La Réunion** by **Virginie Durand**, Pauline Le Bouteiller, Anne Mangeney, El Hadji Koné, Antoine Protin, Philippe Kowalski, Frédéric Lauret, Christophe Brunet, Kerstin Wegner, Florian Haas, and Arthur Delorme

09:00–09:15 EGU2016-2538 **Continuous monitoring of shear wave velocity at the Montevecchio earthflow (Forlì-Cesena Province, Northern Apennines)** by **Lara Bertello**, Matteo Berti, and Silvia Castellaro

09:15–09:30 EGU2016-15705 **Automatic classification of endogenous seismic sources within a landslide body using random forest algorithm** by **Floriane Provost**, Clément Hibert, Jean-Philippe Malet, André Stumpf, and Cécile Doubre

09:30–09:45 EGU2016-11130 **Testing the seismology-based landquake monitoring system** by **Wei-An Chao**

09:45–10:00 EGU2016-14618 **High-speed landslide mechanism extracted from long-period surface waves** by **Juan Zhao**

WE2, 10:30–12:00

NH3.3/SSS12.28, Characterizing and monitoring landslide processes using remote sensing and geophysics (co-organized), **Orals**, **10:30–10:45**, **Room N2**

10:30–10:45 EGU2016-12505 **Exploring the potential of Sentinel-1 data for regional scale slope instability detection using multi-temporal interferometry** by **Janusz Wasowski**, Fabio Bovenga, Raffaele Nutricato, Davide Oscar Nitti, Maria Teresa Chiaradia, Alberto Refice, and Guido Pasquariello

10:45–11:00 EGU2016-2916 **Potentiality of SENTINEL-1 for landslide detection: first results in the Molise Region (Italy)** by **Anna Barra**, Oriol Monserrat, Paolo Mazzanti, Carlo Esposito, Michele Crosetto, and Gabriele Scarascia Mugnozza

11:00–11:15 EGU2016-13096 **Deformation responses of slow moving landslides to precipitation in the Northern Apennines (Italy).** by **Benedikt Bayer**, Alessandro Simoni, David Schmidt, Lara Bertello, and Matteo Berti

11:15–11:30 EGU2016-12256 **Monitoring landslide kinematics by multi-temporal radar interferometry - the Corvara landslide case study** by **Benni Thiebes**, Giovanni Cuozzo, Mattia Callegari, Romy Schlögel, Marco Mulas, Alessandro Corsini, and Volkmar Mair

11:30–11:45 EGU2016-5255 **Potential Deep Seated Landslide Mapping from Various Temporal Data – Benchmark, Aerial Photo, and SAR** by **Kuo-Lung Wang**, Jun-Tin Lin, Yi-Hsuan Lee, Meei-Ling Lin, Chao-Wei Chen, Ray-Tang Liao, Chung-Chi Chi, and Hsi-Hung Lin

11:45–12:00 EGU2016-12846 **Grouped frequent sequential patterns derived from terrestrial image time series to monitor landslide behaviour – Application to the dynamics of the Sanières/Roche Plombée rockslide.** by Youen Péricault, Catherine Pothier, Nicolas Méger, Emmanuel Trouvé, Flavien Vernier, Christophe Rigotti, and **Jean-Philippe Malet**

WE3, 13:30–15:00

HS5.2, Water resources - assessment, management, and allocation - in (semi-)arid regions, **Orals**, **13:45–14:00**, **Room B**

HS9.1/GM9.7/SSS12.29, Measurement and monitoring techniques for evaluating sediment transport and dynamic processes in open-water environments (co-organized), **Orals**, **13:30–13:45**, **Room 2.44**

	14:30–14:45 EGU2016-17016 **Enhanced detection of water and ground surface in airborne laser bathymetry data using waveform stacking** by **Andreas Roncat** and Gottfried Mandlburger
	NH1.1, Extreme meteorological and hydrological events induced by severe weather and climate change, **Orals**, **13:30–13:45**, **Room N2** 14:00–14:15 EGU2016-12885 **Extreme floods in the Mekong River Delta under climate change: combined impacts of upstream hydrological changes and sea level rise** by **Long Hoang**, Dung Nguyen Viet, Matti Kummu, Hannu Lauri, Jorma Koponen, Michelle T.H. van Vliet, Iwan Supit, Rik Leemans, Pavel Kabat, and Fulco Ludwig 14:15–14:30 EGU2016-14605 **Statistical characteristics of mudflows in the piedmont areas of Uzbekistan and the role of the synoptic processes for the formation of mudflows** by **Gavkhar Mamadjanova** and Gregor C Leckebusch
WE4, 15:30–17:00	**HS5.2**, Water resources - assessment, management, and allocation - in (semi-)arid regions, **Orals**, **15:45–16:00**, **Room B** 16:30–16:45 EGU2016-16436 **Monitoring small reservoirs in semi-arid region by satellite SAR data** by **Maria Nicolina Papa**, Francesco Mitidieri, Donato Amitrano, Giuseppe Ruello, Gerardo Di Martino, Antonio Iodice, and Daniele Riccio
	HS9.1/GM9.7/SSS12.29, Measurement and monitoring techniques for evaluating sediment transport and dynamic processes in open-water environments (co-organized), **Orals**, **15:30–15:45**, **Room 2.44**
WE5, 17:30–19:00	**GI2.5**, Sentinel 1 for Science, INSAR results, **Posters**, **08:00–19:30**, **Hall A** A.409 EGU2016-828 **Interseismic accumulation across the Khoy fault from InSAR measurement** by **Mohammad Mohseni Aref**, Ziyadin Çakir, and Sadra Karimzadeh A.410 EGU2016-1987 **Preliminary Study of Ground Movement in Prone Landslide Area by Means of MAI InSAR A Case Study: Ciloto, West Java, Indonesia** by **Noorlaila Hayati**, Björn Riedel, and Wolfgang Niemeier A.411 EGU2016-2581 **TerraSAR-X time-series interferometry detects human-induce subsidence in the Historical Centre of Hanoi, Vietnam** by **Tuan Le**, Chung-Pai Chang, and Xuan Nguyen A.413 EGU2016-13714 **2D Modelling of the Gorkha earthquake through the joint exploitation of Sentinel 1-A DInSAR measurements and geological, structural and seismological information** by **Vincenzo De Novellis**, Raffaele Castaldo, Giuseppe Solaro, Claudio De Luca, Susi Pepe, Manuela Bonano, Francesco Casu, Ivana Zinno, Michele Manunta, Riccardo Lanari, and Pietro Tizzani A.414 EGU2016-13875 **Groundwater storage variations in Madrid (Central Spain) from InSAR data** by **Marta Béjar-Pizarro**, Pablo Ezquerro, Gerardo Herrera, Roberto Tomás, Carolina Guardiola-Albert, Jose M. Ruiz-Hernandez, Jose A. Fernandez-Merodo, Miguel Marchamalo, and Ruben Martinez A.415 EGU2016-13957 **A Copernicus downstream service for surface displacement monitoring in Germany** by **Andre Cahyadi Kalia**, Michaela Frei, and Thomas Lege A.416 EGU2016-14057 **Persistent Scatterer Interferometry based detection of strong subsidence in Semarang, Indonesia** by **Andre Cahyadi Kalia** A.418 EGU2016-14891 **Long-term and wide-area subsidence pattern from time series of Envisat Asar Data in Konya Basin, Turkey** by **Aydin Ustun**

A.419 EGU2016-16523 **A NRT Sentinel-1 processing paradigm towards the implementation of a Persistent Scatterers Journal (withdrawn)** by **Charalampos Kontoes**, Ioannis Papoutsis, Themistocles Herekakis, Christina Psychogiou, Nikos Svigkas, and Maria Kaskara

A.420 EGU2016-16836 **Comparison of COSMO-SkyMed PSP SAR interferometry ground deformation analysis with field measurements and geological studies: the case study of Wuhan city (withdrawn)** by **Mario Costantini**, Jie Bai, Jianhua Xiao, Fabio Malvarosa, Federico Minati, Francesco Vecchioli, Qiong Hu, and Jiping Li

A.421 EGU2016-16974 **InSAR measurements for the 2014 Mw 6.0 Jinggu, Yunnan Earthquake** by **Jiajun Chen**, Wanpeng Feng, Samsonov Sergey, Motagh Mahdi, Zhenhong Li, and Peter Clarke

GMPV5.3/G3.8/GD8.8/TS2.6, Volcanic processes: Tectonics, Deformation, Geodesy (co-organized), **Posters**, **08:00–19:30**, **Hall X2**

HS5.2, Water resources - assessment, management, and allocation - in (semi-)arid regions, **Posters**, **08:00–19:30**, **Hall A**

HS9.1/GM9.7/SSS12.29, Measurement and monitoring techniques for evaluating sediment transport and dynamic processes in open-water environments (co-organized), **Posters**, **08:00–19:30**, **Hall A**

NH1.1, Extreme meteorological and hydrological events induced by severe weather and climate change, **Posters**, **08:00–19:30**, **Hall D**

NH3.3/SSS12.28, Characterizing and monitoring landslide processes using remote sensing and geophysics (co-organized), **Posters**, **08:00–19:30**, **Hall D**

D.50 EGU2016-7513 **Active and passive seismic methods for characterization and monitoring of unstable rock masses: field surveys, laboratory tests and modeling.** by Chiara Colombero, Laurent Baillet, Cesare Comina, Denis Jongmans, and **Sergio Vinciguerra**

D.51 EGU2016-15246 **Contribution of a 3D velocity model and of beam forming method for the location of microseismic sources generated in soft rock landslides** by **Floriane Provost**, Jean-Philippe Malet, Agnès Helmstetter, Cécile Doubre, and Julien Gance

D.52 EGU2016-8332 **Seismic detection and characterization of gravitational mass movements** by **Florian Fuchs**, Wolfgang Lenhardt, and Götz Bokelmann

D.53 EGU2016-13806 **Deformation analysis for understanding landslide-induced brittle fractures at the Super-Sauze landslide** by **Sabrina Rothmund**, Rolf Häfner, and Manfred Joswig

D.54 EGU2016-2350 **Geophysical investigation of landslides and fault scarps in the Hockai Fault Zone, Belgium** by **Anne-Sophie Mreyen**, Hans-Balder Havenith, and Tomas Fernandez-Steeger

D.55 EGU2016-5958 **Seismic monitoring of soft-rock landslides: New case study at Pechgraben mudslide - Upper Austria** by **Naomi Vouillamoz**, Juan Carlos Santoyo, David Ottowitz, Birgit Jochum, Stefan Pfeiler, Robert Supper, and Manfred Joswig

D.56 EGU2016-3724 **Landslides on salt deposits - monitoring with electrometry** by Ovidiu Avram and **Emil Rusu**

D.57 EGU2016-13308 **Hydrological Interpretation of ERT Monitoring Data on active landslides by implementation of numerical modelling at sites of the LAMOND Long-Term Landslide Monitoring Network** by **Stefan Hoyer**, David Ottowitz, Robert Supper, Birgit Jochum, Monika Riegler, Anna Scolobig, and Stefan Pfeiler

D.58 EGU2016-5583 **Geophysical measurements and monitoring on the Pechgraben Landslide in Upper Austria** by **Birgit Jochum**, David Ottowitz, Stefan Pfeiler, Stefanie Gruber, Stefan Hoyer, Robert Supper, and Ingrid Schattauer

D.59 EGU2016-2790 **The low-cost GNSS GEOMON system for monitoring landslide displacements** by Michel Demierre, **Jean-Philippe Malet**, Laurent Folladore, Pierre Boetzlé, Jeanneret Martin, Gilbert Ferhat, and Patrice Ulrich

D.60 EGU2016-7886 **The Salcher landslide observatory: a new long-term monitoring site in Austria** by **Ekrem Canli**, Alexander Engels, Thomas Glade, Joachim Schweigl, and Michael Bertagnoli

D.61 EGU2016-13310 **Two potential cases of earthquake-induced landslides in Vrancea Seismic Region (Romania)** by **Mihai Micu**, Dan Balteanu, Hans-Balder Havenith, Alexandru Onaca, and Carmen Cioflan

D.62 EGU2016-3927 **Multi-temporal InSAR monitoring of landslides in a tropical urban environment: focus on Bukavu (DR Congo)** by **Adriano Nobile**, Elise Monsieurs, Olivier Dewitte, Nicolas d'Oreyes, and Francois Kervyn

D.63 EGU2016-10841 **Testing the potential of Sentinel-1 TOPS interferometry for the detection and monitoring of landslides at local scale** by **Simone Fiaschi**, Matteo Mantovani, Simone Frigerio, Gianluca Marcato, Alessandro Pasuto, and Mario Floris

D.64 EGU2016-11739 **Preliminary assessment of active rock slope instabilities in the high Himalaya of Bhutan** by **Benedetta Dini**, Andrea Manconi, Kerry Leith, and Simon Loew

D.65 EGU2016-2218 **Investigation of deep gravitational slope deformation by time-series InSAR combined with photogeological and geomorphological analysis** by **Yi Zhang**, Xingmin Meng, Guan Chen, Liang Qiao, Yinyin Xu, and Jing Chang

D.66 EGU2016-14765 **Landslide movement mapping by sub-pixel amplitude offset tracking – case study from Corvara landslide** by Mehdi Darvishi, **Romy Schlögel**, Giovanni Cuozzo, Mattia Callegari, Benni Thiebes, Lorenzo Bruzzone, Marco Mulas, Alessandro Corsini, and Volkmar Mair

D.67 EGU2016-14177 **Landslides hazard mapping integrating remote sensing and geo-morphological data in the Sorrentina Peninsula coastal areas** by **claudia spinetti**, marina bisson, cristiano tolomei, laura colini, alessandro galvani, marco moro, michele saroli, and vincenzo sepe

D.68 EGU2016-2361 **Multi-stage evolution process of large scale landslides at the Patanpunas stream, Taiwan** by Ming-Lang Lin, Kuo-Chen Lee, **Chia-Ming Lo**, Meng-Chia Weng, and Shun-Min Lee

D.69 EGU2016-8428 **Application of Digital Image Correlation Method to Improve the Accuracy of Aerial Photo Stitching** by **Shih-Heng Tung**, You-Liang Jhou, Ming-Hsiang Shih, Han-Wei Hsiao, and Wen-Pei Sung

D.70 EGU2016-520 **Object-based Landslide Mapping: Examples, Challenges and Opportunities** by **Daniel Hölbling**, Clemens Eisank, Barbara Friedl, Kang-Tsung Chang, Tsai-Tsung Tsai, Gro Birkefeldt Møller Pedersen, Harley Betts, Francesca Cigna, Shou-Hao Chiang, Benjamin Aubrey Robson, Silvia Bianchini, Petra Füreder, Florian Albrecht, Raphael Spiekermann, Elisabeth Weinke, Thomas Blaschke, and Chris Phillips

D.71 EGU2016-7742 **Precision Improvement of Photogrammetry by Digital Image Correlation** by **Ming-Hsiang Shih**, Wen-Pei Sung, Shih-Heng Tung, and Hanwei Hsiao

D.72 EGU2016-3976 **Monitoring the Lavina di Roncovetro (RE, Italy) landslide by integrating traditional monitoring systems and multiple high-resolution topographic datasets** by **Alessandro Fornaciai**, Massimiliano Favalli, Giovanni Gigli, Luca Nannipieri, Lorenzo Mucchi, Emanuele Intieri, Andrea Agostini, Marco Pizziolo, Giovanni Bertolini, Federico Trippi, Nicola Casagli, Rosa Schina, and Ennio Carnevale

D.73 EGU2016-9511 **An integrated management tool for rockfall evaluation along transportation corridors: the ParaChute research project** by Catherine Cloutier, Jacques Locat, **Mélanie Mayers**, François Noël, Dominique Turmel, Chantal Jacob, Pierre Dorval, François Bossé, Pierre Gionet, and Michel Jaboyedoff

D.74 EGU2016-12476 **Analysis with SfM on-motion method of July 2015 extreme rainfall impacts on the S-charl valley road in the Canton of Graubünden, Switzerland** by **Jérémie Voumard** and Michel Jaboyedoff

D.75 EGU2016-12886 **Terrestrial Laser Scanner for assessing rockfall susceptibility in the Cilento rocky coast (Southern Italy)** by **Valerio Sorrentino**, Battista Matasci, Antonio Abellan, Michel Jaboyedoff, Ermanno Marino, Antonio Pignalosa, and Antonio Santo

D.76 EGU2016-15666 **Characterization and monitoring of the Séchilienne rock slope using 3D imaging methods (Isère, France)** by **Cindy Vulliez**, Antoine Guerin, Antonio Abellán, Marc-Henri Derron, Michel Jaboyedoff, Marie-Aurélie Chanut, Laurent Dubois, and Jean-Paul Duranthon

Thursday, 21 April

TH1, 08:30–10:00

GMPV5.3/G3.8/GD8.8/TS2.6, Volcanic processes: Tectonics, Deformation, Geodesy (co-organized), **Orals**, **08:30–08:45**, **Room L6**

NH3.14/GM8.12/SSS2.29, Rockfalls, rockslides and rock avalanches (co-organized), **Orals**, **08:30–08:45**, **Room L3**

08:45–09:00 EGU2016-7528 **Approaching a more Complete Picture of Rockfall Activity: Seismic and LiDAR Detection, Loaction and Volume Estimates** by **Michael Dietze**, Solmaz Mohadjer, Jens Turowski, Todd Ehlers, and Niels Hovius

TH2, 10:30–12:00

GMPV5.3/G3.8/GD8.8/TS2.6, Volcanic processes: Tectonics, Deformation, Geodesy (co-organized), **Orals**, **10:30–10:45**, **Room L6**

10:30–10:45 EGU2016-3113 **Using InSAR to investigate long term caldera unrest: case studies from Yellowstone and Long Valley** by **maurizio battaglia**

NH3.14/GM8.12/SSS2.29, Rockfalls, rockslides and rock avalanches (co-organized), **Orals**, **10:30–10:45**, **Room L3**

TH3, 13:30–15:00

GMPV5.3/G3.8/GD8.8/TS2.6, Volcanic processes: Tectonics, Deformation, Geodesy (co-organized), **Orals**, **13:30–13:45**, **Room L6**

13:45–14:00 EGU2016-12555 **Volcano-tectonic deformation in the Kivu Region, Central Africa: Results from multi-year InSAR time series analysis and continuous GNSS observations of the Kivu Geodetic Network (KivuGNet)** by **Halldor Geirsson**, Nicolas D'Oreye, Benoît Smets, Adriano Nobile, Sergey Samsonov, Dominique De Rauw, Niche Mashagiro, and Francois Kervyn

NH6.1, Application of remote sensing and Earth-observation data in natural hazard and risk studies, **Orals**, **13:30–13:45**, **Room N2**

13:30–13:45 EGU2016-3737 **Preliminary remote sensing assessment of the catastrophic avalanche in Langtang Valley induced by the 2015 Gorkha earthquake, Nepal** by **Hiroto Nagai**, Manabu Watanabe, and Naoya Tomii

13:45–14:00 EGU2016-1032 **Vulnerability assessment of Glacial Lake Outburst Floods using Remote Sensing and GIS in North Sikkim (India), Eastern Himalaya** by **Suruchi Aggarwal**, Juna Probha Devi, Praveen Kumar Thakur, and Suresh Chand Rai

14:00–14:15 EGU2016-4928 **Improving the extraction of crisis information in the context of flood, fire, and landslide rapid mapping using SAR and optical remote sensing data** by **Sandro Martinis**, Stephen Clandillon, André Twele, Claire Huber, Simon Plank, Jérôme Maxant, Wenxi Cao, Mathilde Caspard, and Stéphane May

14:15–14:30 EGU2016-15409 **Dikes under Pressure – Monitoring the Vulnerability of Dikes by Means of SAR Interferometry** by **Philip Marzahn**, Moritz Seidel, and Ralf Ludwig

14:30–14:45 EGU2016-15986 **Exploitation of amplitude and phase of satellite SAR images for landslide mapping: the case of Montescaglioso (South Italy)** by Federico Raspini, Andrea Ciampalini, Luca Lombardi, Massimiliano Nocentini, Giovanni Gigli, Nicola Casagli, **Sara Del Conte**, and Alessandro Ferretti

14:45–15:00 EGU2016-11264 **Probabilistic drought intensification forecasts using temporal patterns of satellite-derived drought indicators** by **Sumin Park**, Jungho Im, and Seonyeong Park

TH4, 15:30–17:00

NH6.3/SSS12.27, The use of Remotely Piloted Aircraft Systems (RPAS) in monitoring applications and management of natural hazards (co-organized), **Orals**, **15:30–15:45**, **Room N2**

16:00–16:15 EGU2016-6489 **Input of UAV, DTM photo-interpretation and SAR interferometry on active tectonics applied on the Southern Coastal Range (SE Taiwan)** by **Benoit Deffontaines**, Kuo-Jen Chang, Johann Champenois, Samuel Magalhaes, and Gregory Serries

	NH9.4, Natural hazard impacts on technological systems and urban areas, **Posters**, **08:00–19:30**, **Hall D**
TH5, 17:30–19:00	**NH3.14/GM8.12/SSS2.29**, Rockfalls, rockslides and rock avalanches (co-organized), **Posters**, **08:00–19:30**, **Hall D**
	NH6.1, Application of remote sensing and Earth-observation data in natural hazard and risk studies, **Posters**, **08:00–19:30**, **Hall D** D.102 EGU2016-8477 **Spatial data integration for analyzing the dynamics of Albanian Adriatic shoreline** by **Luan Arapi**, Pal Nikolli, and Sander Kovaçi D.103 EGU2016-3748 **Emergency satellite observation and assessment of a glacier lake outburst flood in Bhutan** by **Hiroto Nagai**, Takeo Tadono, and Shinichi Suzuki D.104 EGU2016-11243 **Agricultural drought assessment at spatial and temporal scales using remotely sensed data** by **Yongchul Shin**, Kyungwon Park, Jinyoung Rhee, and Sunkwon Yoon D.105 EGU2016-3281 **Shoreline to Height (S2H): an algorithm to monitor reservoirs' water height from satellite images. A flood risk management application** by **Luca Cenci**, Giorgio Boni, Luca Pulvirenti, Simone Gabellani, Fabio Gardella, Giuseppe Squicciarino, Nazzareno Pierdicca, and Catia Benedetto D.106 EGU2016-5236 **Precisely determined the surface displacement by the ionospheric mitigation using the L-band SAR Interferometry over Mt.Baekdu** by **Won-Jin Lee**, Hyung-Sup Jung, Sun-Cheon Park, and Duk Kee Lee D.107 EGU2016-16243 **Space Borne and Ground Based InSAR Data Integration: The Åknes Test Site** by **Federica Bardi**, Federico Raspini, Andrea Ciampalini, Lene Kristensen, Line Rouyet, Tom Rune Lauknes, Regula Frauenfelder, and Nicola Casagli D.108 EGU2016-17631 **Estimated Post-Flood Effects Through Sentinel And Landsat Data to Support Civil Protection (withdrawn)** by **Mariano Focareta**, Nicomino Fiscante, Cesario Vincenzo Angelino, and Luca Cicala D.109 EGU2016-15188 **Application of multi-temporal landform analysis in landslide susceptibility assessment for mountainous highway - a case study in southeastern Taiwan** by **Jian Liu-Xuan**, Huang Wei-Kai, and Lin Po-Shen D.110 EGU2016-3346 **Estimation on rubber tree disturbance caused by typhoon Damery (200518) with Landsat and MODIS data in Hainan Island of China** by **Chenyan Tan**, Weihua Fang, and Jian Li D.111 EGU2016-7653 **Developing scenarios to assess future landslide risks: a model-based approach applied to mountainous regions** by **Laure Vacquie** and Thomas Houet D.112 EGU2016-1743 **A Multihazard Regional Level Impact Assessment for South Asia** by **Giriraj Amarnath**, Niranga Alahacoon, Pramod Aggarwal, and Vladimir Smakhtin D.113 EGU2016-11096 **Development of flood monitoring system using satellite data and geographic information system** by **Kyungwon Park**, Sangmin Jang, Seongkyu Lee, Sunkwon Yoon, and Yongchul Shin D.114 EGU2016-15293 **The drought impact on satellite solar-induced chlorophyll fluorescence in China during 2007-2015** by **Ruitao Li** D.115 EGU2016-17813 **Globally referenced real time monitoring of mass movements using monoscopic time-lapse photography.** by **Robert Kenner**, Marcia Phillips, and Manfred Buchroithner D.116 EGU2016-13331 **Sediment Transportation Induced by Deep-Seated Landslides in a Debris Flow Basin in Taiwan** by **Meei Ling Lin**, Te Wei Chen, Yong Sheng Chen, and Han Sin Jhuang

	D.117 EGU2016-13393 **A fully automatic tool to perform accurate flood mapping by merging remote sensing imagery and ancillary data** by **Annarita D'Addabbo**, Alberto Refice, Francesco Lovergine, and Guido Pasquariello D.118 EGU2016-11290 **Damage and loss assessment on rubber trees caused by typhoon based on high-precision remote sensing data and field investigation** by **Jian Li**, Weihua Fang, and Chenyan Tan D.119 EGU2016-11297 **Differentiation of debris flow deposits through image classification of Landsat 8 images in Nueva Ecija after Typhoon Koppu (withdrawn)** by **Carmille Marie Escape** D.120 EGU2016-8770 **Forecast-based Integrated Flood Detection System for Emergency Response and Disaster Risk Reduction (Flood-FINDER)** by Mauro Arcorace, Francesco Silvestro, Roberto Rudari, **Giorgio Boni**, Luca Dell'Oro, and Einar Bjorgo
	NH6.3/SSS12.27, The use of Remotely Piloted Aircraft Systems (RPAS) in monitoring applications and management of natural hazards (co-organized), **Posters**, **08:00–19:30**, **Hall D**
TH5, 17:30–19:00	**NH9.4**, Natural hazard impacts on technological systems and urban areas, **Orals**, **17:30–17:45**, **Room N2** 17:30–17:45 EGU2016-1500 **Heavy Precipitation impacts and emergency planning – developing applicable strategies for a metropolitan area** by **Thomas Kutschker** and Thomas Glade 17:45–18:00 EGU2016-1545 **Risk prediction of Critical Infrastructures against extreme natural hazards: local and regional scale analysis** by **Vittorio Rosato**, Micheline Hounjet, Andreas Burzel, Antonio Di Pietro, Alberto Tofani, Maurizio Pollino, and Sonia Giovinazzi 18:00–18:15 EGU2016-15356 **Sustainable regional development and natural hazard impacts** by **Elena Petrova**, Vladimir Svetlosanov, and Valery Kudin

附錄 2

報告論文及簡報

（此會議僅需提供摘要、簡報或海報）

Geophysical Research Abstracts
Vol. 18, EGU2016-5255-1, 2016
EGU General Assembly 2016

Potential Deep Seated Landslide Mapping from Various Temporal Data – Benchmark, Aerial Photo, and SAR

Kuo-Lung Wang (1), Jun-Tin Lin (1), Yi-Hsuan Lee (1), Meei-Ling Lin (2), Chao-Wei Chen (3), Ray-Tang Liao (3), Chung-Chi Chi (4), and Hsi-Hung Lin (4)

(1) Civil Engineering, National Chi Nan University, Nantou, Taiwan (klwang@ncnu.edu.tw), (2) Civil Engineering, National Taiwan University, Taipei, Taiwan, (3) Safe Engineering Consultant, Taipei, Taiwan, (4) Central Geological Survey, Ministry of Economic Affairs, Taipei, Taiwan

Landslide is always not hazard until mankind development in highly potential area. The study tries to map deep seated landslide before the initiation of landslide. Study area in central Taiwan is selected and the geological condition is quite unique, which is slate. Major direction of bedding in this area is northeast and the dip ranges from 30-75 degree to southeast. Several deep seated landslides were discovered in the same side of bedding from rainfall events. The benchmarks from 2002 $\sim$ 2009 are in this study. However, the benchmarks were measured along Highway No. 14B and the road was constructed along the peak of mountains. Taiwan located between sea plates and continental plate. The elevation of mountains is rising according to most GPS and benchmarks in the island. The same trend is discovered from benchmarks in this area. But some benchmarks are located in landslide area thus the elevation is below average and event negative. The aerial photos from 1979 to 2007 are used for orthophoto generation. The changes of land use are obvious during 30 years and enlargement of river channel is also observed in this area. Both benchmarks and aerial photos have discovered landslide potential did exist this area but how big of landslide in not easy to define currently. Thus SAR data utilization is adopted in this case. DInSAR and SBAS sar analysis are used in this research and ALOS/PALSAR from 2006 to 2010 is adopted. DInSAR analysis shows that landslide is possible mapped but the error is not easy to reduce. The error is possibly form several conditions such as vegetation, clouds, vapor, etc. To conquer the problem, time series analysis, SBAS, is adopted in this research. The result of SBAS in this area shows that large deep seated landslides are easy mapped and the accuracy of vertical displacement is reasonable.

Potential Deep Seated Landslide Mapping from Various Temporal Data – Benchmark, Aerial Photo, and SAR

Jun-Ting LIN I-Hsuan LEE	Meei-Ling LIN	Chai-Wei CHEN Ray-Tang LIAO	Chung-Chi CHI Hsi-Hung LIN
National Chi Nan University	National Taiwan University	Safe Consultant Co.	Central Geological Survey

1

Study area

2

Study Flow

1979-2007	• Aerial Photos • Benchmark
2007-2010	• Benchmark • SAR (ALOS/PALSAR)
Currently	• SAR (ALOS2/PALSAR, Sentinel 1, Terra-X, etc) • UAS with high precision GPS GCPs

3

Events recently (within ALOS/PALSAR life)

Years	Event
2007	Sepat, Krosa, Wipha
2008	Kalmaegi, Fung-wong, Jangmi, Sinalu
2009	Molave, Morakot, Parma
2010	Heavy Rainfall, Lionrock, Namtheun, Meranti, Fanapi, Megi

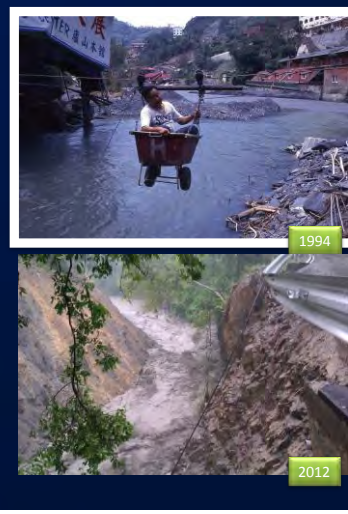

Previous landslide mapping w/ LiDAR

- Scars were mapped from 2010~2012 in study area (Central Geological Survey, 2010; 2011; 2012)
- Scars show previous landslide event but can not provide evidence for sliding velocity

5

Benchmark observation – 2002~2009

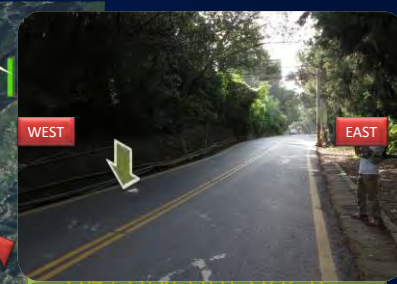

conducted for average uplift in study area

- Value lower than average means relative lower elevation, which means located in landslide area

6

Eliminate uplift effect of plate

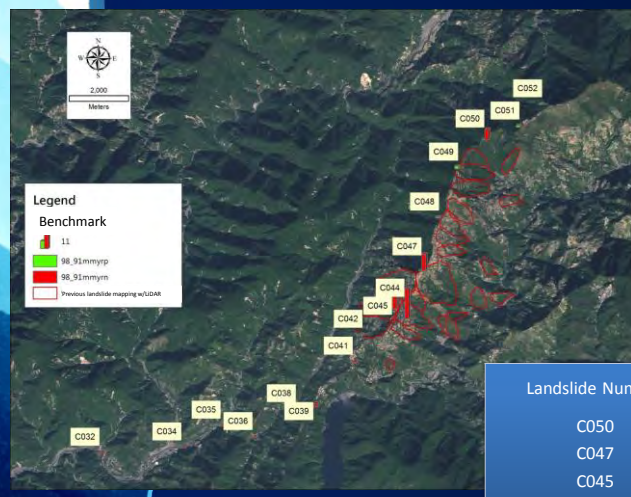

- Normalized with years (mm/year)
- Green means up
- Red means down

Landslide Number	Relative decreasing velocity (mm/year)
C050	8.02
C047	12.03
C045	9.90
C044	22.06

7

Orthophoto and Digital Surface Model Generation

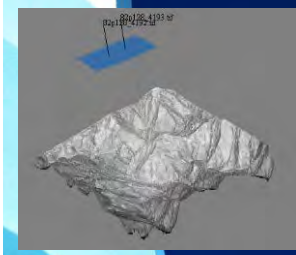

Aerial Photos

Overlap selection | GCP candidate

↓

Google Earth Location

GCP candidate | Field precise GPS survey

↓

Aerotriangulation and Generate Dense Point Clouds

Orthophoto | DSM

8

28 years differences

1979

2007

Product resolution with GCPs found
Ortho: 0.4~1.2 m
DSM: 1.6~4.5 m

9

Orthophoto (1979~2007)

10

Hillshade (1979~2007)

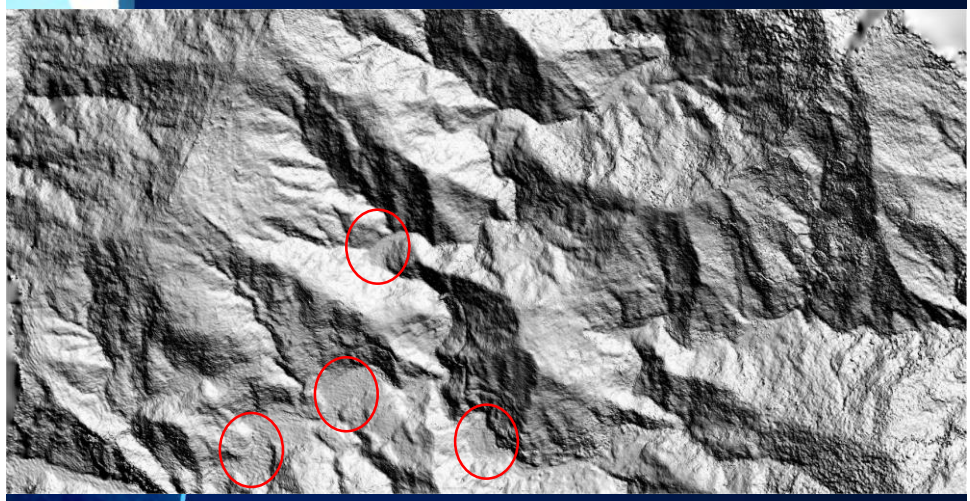

Slope Angle (1979~2007)

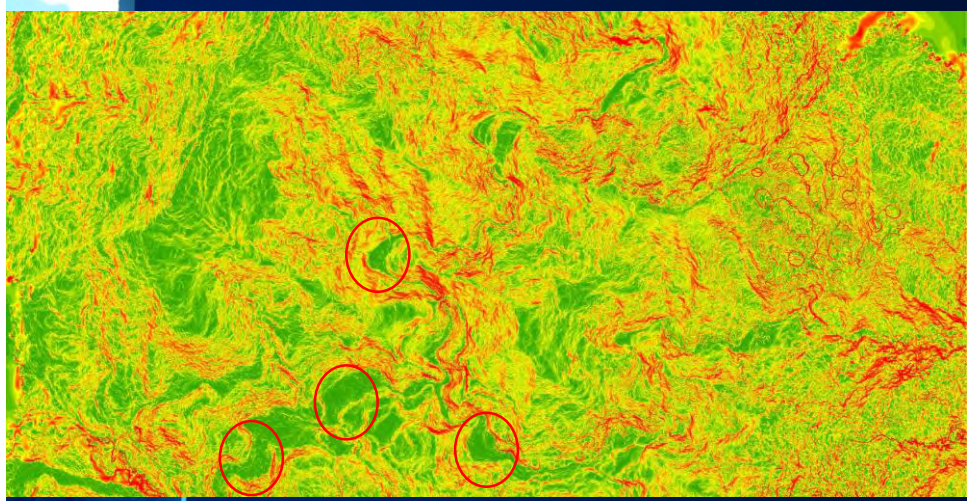

Building displacement near Guest House

2015 (UAS)

13

Differential Interferometric Synthetic Aperture Radar (DInSAR)

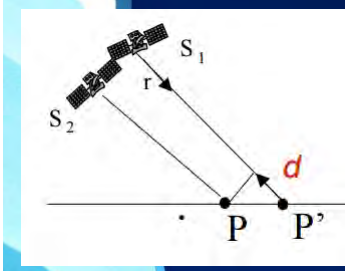

F Rocca(2007)

- Slightly deformation of LoS (d) and radar phase difference

$$\Delta\varphi_{displacement} = \frac{4\pi}{\lambda} d$$

- LoS is including uplift of plate
  - → solution: minus average uplift from benchmark
  - →real slope deformation
- ALOS/PALSAR from 2007 to 2009

14

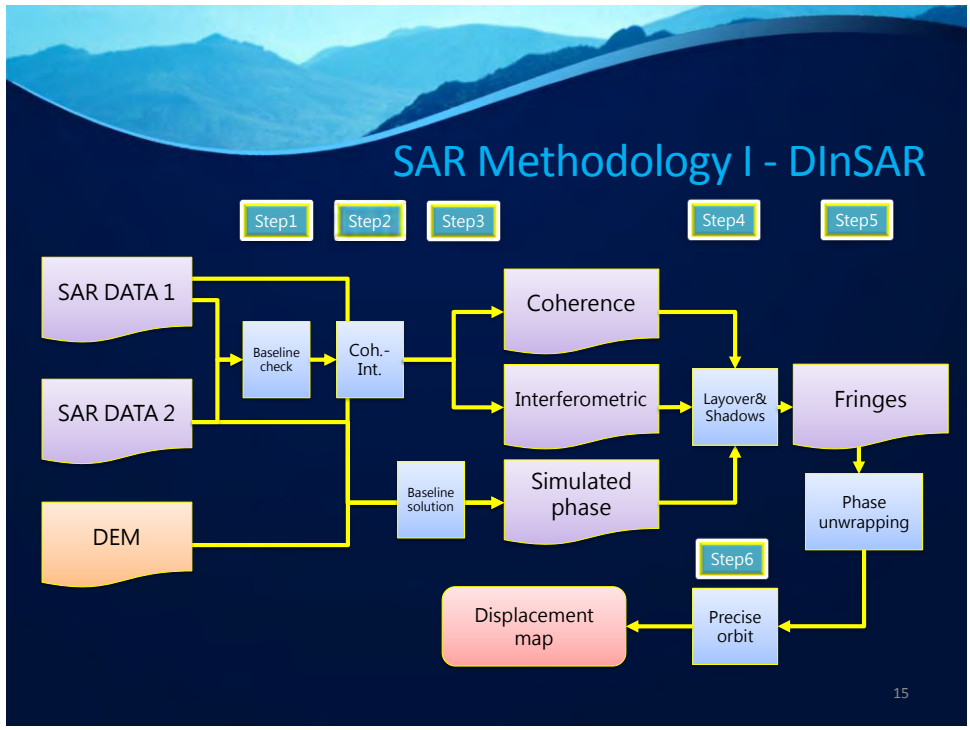
SAR Methodology I - DInSAR
Step1
Step2
Step3
Step4
Step5
SAR DATA 1
SAR DATA 2
DEM
Baseline check
Coh.-Int.
Baseline solution
Coherence
Interferometric
Simulated phase
Layover& Shadows
Fringes
Phase unwrapping
Step6
Precise orbit
Displacement map
15

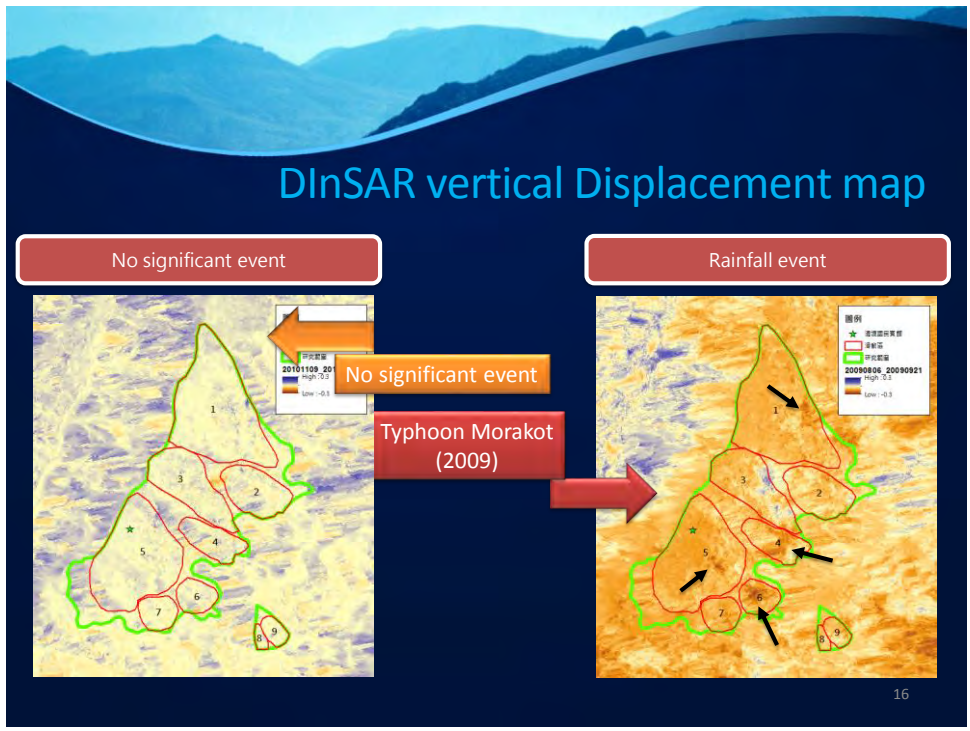
DInSAR vertical Displacement map
No significant event
Rainfall event
No significant event
Typhoon Morakot (2009)
16

SAR Methodology II - Interferometric Stacking

PS (Persistent Scatterers)	SBAS (Small Baseline Subset)
Independent, incorrelated motions	At best spatially correlated motions ✓
Pixel wise continuous time series ✓	Possibility of handling time series with temporal holes
Time interval between two acquisitions limited by displacement rate	Time interval between two acquisitions limited by temporal decorrelation ✓
Very accurate on PS ✓	Slightly less accurate
Linear displacements favoured	Larger variety of parametric models possible. Non-parametric modeling possible ✓

17

PS-InSAR result

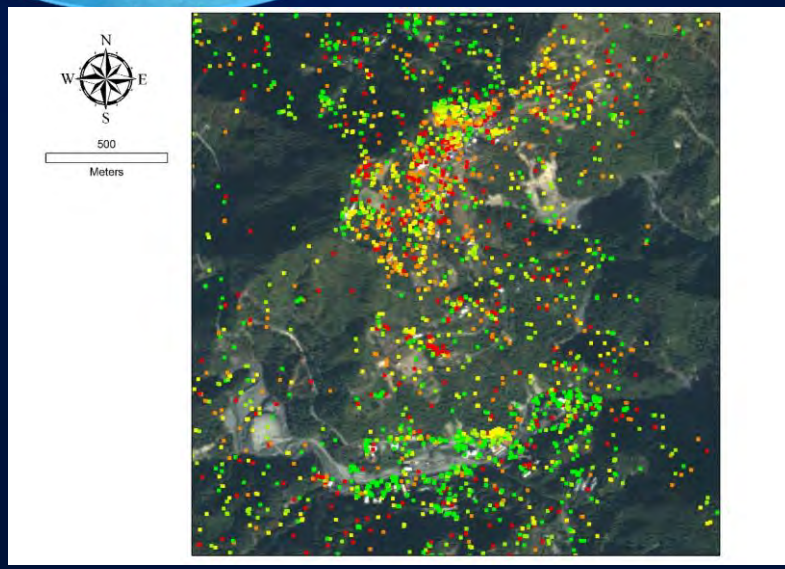

18

SBAS analysis result

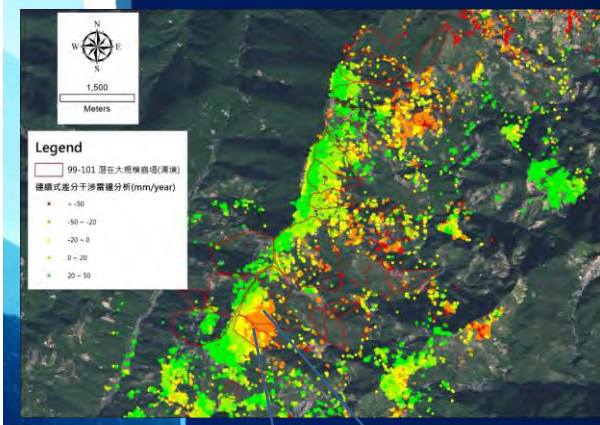

- Average vertical accuracy is 9.4 mm/year with 3.2 mm/year standard deviation
- Relative velocity of benchmark C044 is 22.06 mm/year going down
- Relative velocity of benchmark C044 from SBAS is 22.20mm/year doing down
- No data solved of the other 3 points
- Fastest velocity scars in study area are no. 057 and 063

19

Conclusions and Future Works

- Benchmark can provide information that the points are within landslide scars or not
- Orthophotos produced from aerial photos can provide concept idea of landslide and deposition but not precise deformation value. More accurate data can be found with UAS produced DSM.
- DInSAR and SBAS can not identify relative stable slopes but slide in the past
- SBAS can define moving landslide scars and their velocities, which is suitable for landslide morning

20

Conclusions and Future Works

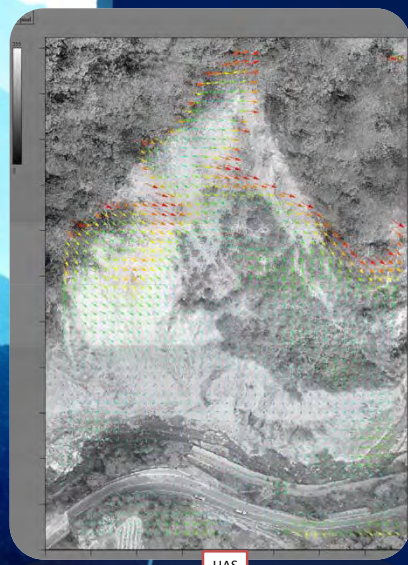

UAS

- Landslide research is a long term work to prevent hazards and maybe have no feedback but needs to keep going and going.

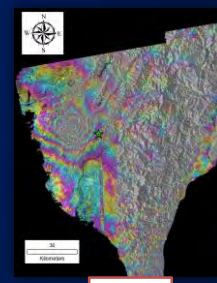

Sentinel 1

21

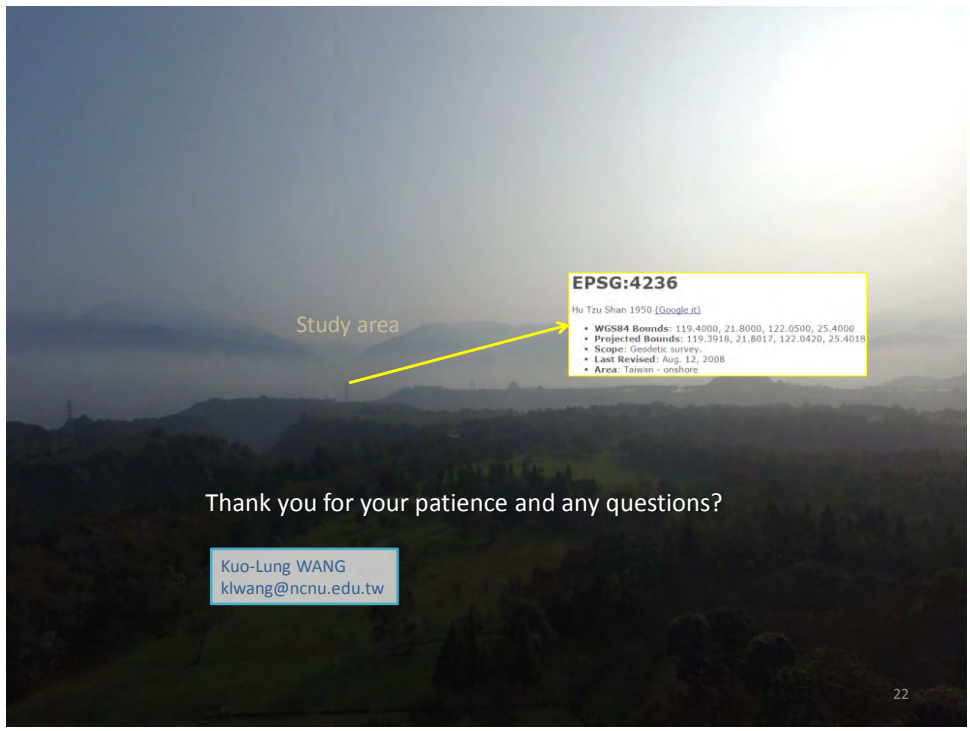

Thank you for your patience and any questions?

Kuo-Lung WANG
klwang@ncnu.edu.tw

22

附錄 3
取得海報縮影

Space-Borne and Ground-Based InSAR Data Integration: The Åknes Test Site

Bardi F.[1*], Raspini F. [1], Ciampalini A. [1], Kristensen L. [2], Rouyet L. [3], Lauknes T. R. [3], Frauenfelder R. [4], Casagli N. [1]

1 Department of Earth Sciences, Università di Firenze, via La Pira 4, 50121 Firenze, Italy; federico.raspini@unifi.it (F.R.); andrea.ciampalini@unifi.it (A.C.); nicola.casagli@unifi.it (N.C.)
2 Norwegian Water Resources and Energy Directorate (NVE), Ødegårdsvegen 176, 6200 Stranda, Norway; lkr@nve.no (L.K.)
3 Norut Northern Research Institute, 9294 Tromsø, Norway; line.rouyet@norut.no (L.R.); tom.rune.lauknes@norut.no (T.R.L.)
4 Norwegian Geotechnical Institute (NGI), Sognsveien 72, 0806 Oslo, Norway; Regula.Frauenfelder@nga.no (R.F.)

* Corresponding author: federica.bardi@unifi.it; Tel.: +39-055-27-7777

1) INTRODUCTION

This work concerns a proposal of integration of InSAR (Interferometric Synthetic Aperture Radar) data acquired by ground-based (GB) and satellite platforms. The selected test site is the Åknes rockslide, which affects the western Norwegian coast. The availability of GB-InSAR and satellite InSAR data and the accessibility of a wide literature make the landslide suitable for testing the proposed procedure. Two datasets, acquired by RADARSAT-2 (related to a period between October 2008 and August 2013) and by a combination of TerraSAR-X and TanDEM-X (acquired between July 2010 and October 2012), both of them in ascending orbit, processed applying SBAS (Small BAseline Subset) method, are available. GB-InSAR data related to five different campaigns of measurements, referred to the summer seasons of 2006, 2008, 2009, 2010 and 2012, are available, as well. Data integration has been performed firstly from a qualitative point of view and later from a semi-quantitative point of view.

2) THE TEST SITE

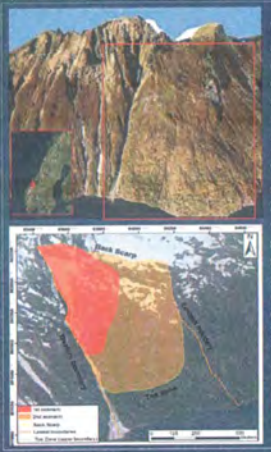

The Åknes rockslide is located in the northwestern side of Sunnylvsfjorden, a branch of the Storfjorden, on the western Norwegian coast. Its location, which develops above the fjord and near several communities, makes the surrounding area exposed to a high level of risk, mainly in terms of a possible tsunami, induced by the collapse of rock material into the fjord (Blikra et al., 2005; Eidsvik et al., 2011).

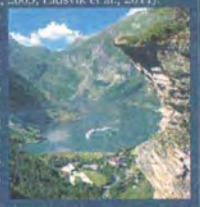

The area also represents one of Norway's most visited tourist attractions, thanks to the natural beauty of the mentioned fjord (the nearby Geirangerfjord is listed on UNESCO's World heritage list).

Two main sectors based on different deformation patterns and consequently different risk scenarios have been identified in the landslide body (Kristensen et al., 2013).

3) METHODS

Data integration is performed during the post-processing phase, and it can be achieved by using a qualitative and/or a semi-quantitative approach.

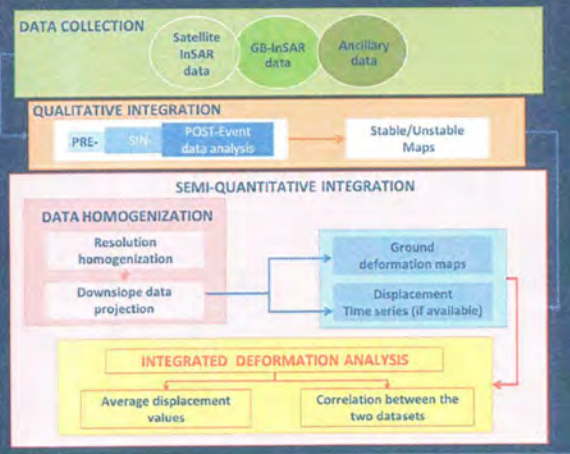

4) GB-InSAR MONITORING ACTIVITY

GB-InSAR FEATURES (Kristensen et al., 2013)	
Rail length	3 m
Central frequency	17.2 GHz
Bandwidth	60 MHz
Number of frequencies	2501
Steps along the rail	601
Image acquisition time	8 min
Processed image range	1800–4200 m
Processed image azimuth	±1200 m
Distance to the back scarp	3000 m

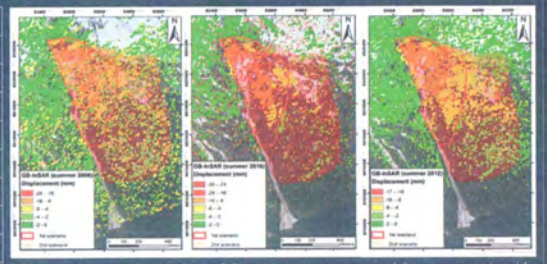

The maps show a quite consistent deformation pattern, measured from year to year with a maximum of 34 mm in about a 4-month interval from July–October 2010.

5) SPACE-BORNE INSAR MONITORING ACTIVITY

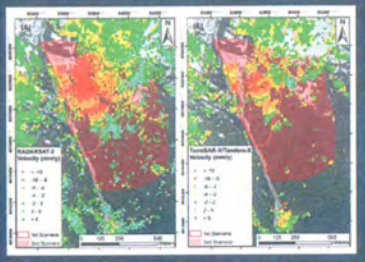

In the case of satellite InSAR acquisitions, two datasets are available, acquired by RADARSAT-2 (14 images) and by a combination of TerraSAR-X and TanDEM-X (13 images), both in ascending orbit, which is the best configuration to avoid layer effects in east-facing slopes' observations. The LOS of both the satellites ranges between 76° and 77° in azimuth and between 25° and 28° in look angle. The RADARSAT-2 dataset includes images acquired between October 2008 and August 2013, with a revisiting time of 24 days; whereas TerraSAR-X/Tandem-X acquisitions are related to a shorter period, between July 2010 and October 2012, with a repeat time of 11 days. Only summer-early autumn periods are meaningful, because in other periods, the snow cover causes interferometric decorrelation (*i.e.*, different scattering properties from one scene to another).

RADARSAT-2 and TerraSAR-X data have been processed applying the SBAS (Small BAseline Subset (Berardino et al., 2002; Lauknes et al., 2011)) method.

6) RESULTS

QUALITATIVE INTEGRATION

Qualitative data integration has been performed in the GIS environment, overlapping all of the available InSAR datasets on the available orthophoto. Data have been classified into two categories, to distinguish stable areas from unstable areas, independent of data type and relative reference period. The stability threshold has been fixed at 2 mm, according to the accuracy of both the GB-InSAR and satellite InSAR technique. The main advantage of this integration step is in the improved density of measurements, which determines an almost complete coverage of the study area. Moreover, the distinction between stable and unstable areas is strongly emphasized

SEMI-QUANTITATIVE INTEGRATION

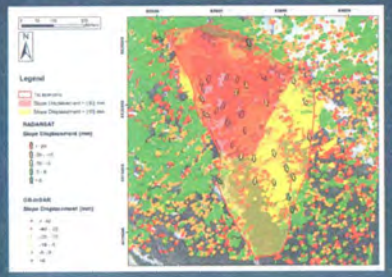

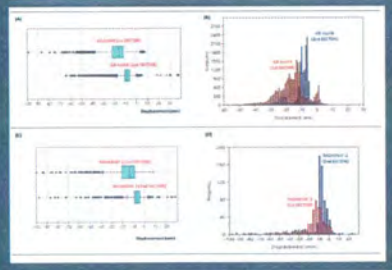

Displacement values, detected by RADARSAT-2 and the GB-InSAR, agree to define the "middle" part of the landslide (defining as "landslide" only the portion of the rockslide, which is included in the limits that define the most dangerous possible scenario) as concerns the major movement, reaching more than 40 mm of displacement in about three months. The upper part of the landslide, mainly affected by vertical displacements, shows displacement values around 5 mm in the downslope direction. A further distinction in two sectors of the first landslide scenario is obtained. The upper part of the scenario (shown in red on the map) represents the area concerning higher displacements, with respect to the lower part (in yellow/on the map). Statistical analysis supports this further distinction.

7) CONCLUSION

In this work, an attempt to integrate ground-based and satellite InSAR datasets is proposed. The main objective is to improve the knowledge obtainable from InSAR techniques, in the field of landslide mapping and monitoring.

The proposed procedure suggests three main steps to be performed: a qualitative phase, the result of which follows a binary approach, with the distinction, in the observed scenario, of stable and unstable areas; a semi-quantitative phase, where the distinction of macro-areas concerning different displacement ranges is possible; a quantitative integration, during which time series analysis is performed, and forecasting algorithms for the evaluation of the future behavior of the landslide can be applied.

The Åknes Norwegian rockslide has been selected to test the proposed procedure.

Firstly, data acquired by satellite and GB-InSAR platforms have been analyzed separately. Data analysis allows one to define landslide sectors concerning higher displacements, which correspond to the upper portion of the slope.

For the application of the integration algorithm, a defined period in the available datasets has been selected. The period between July and October 2010 has been chosen, as it is characterized by the best overlap between ground-based and satellite acquisitions.

The different datasets have been homogenized in terms of spatial and temporal resolution and also as regarding their different LOS.

Data integration allowed increasing the data coverage on the observed scenario, which becomes widely detectable. Data projection allowed better defining of the real value of the displacement vector in the observed scenario: projection reliability has been tested comparing its result with data acquired by GPS campaigns, available in the literature. The projection also allowed defining the upper portion of the landslide as the main vertical displacements of concern.

Data integration from a semi-quantitative point of view has also been performed, allowing proposing the distinction of the upper sector of the landslide, defined as concerning higher displacements, into two sub-sections: the upper portion concerning displacements higher than 10 mm in the period between July and October 2010; and the lower portion concerning displacements lower than 10 mm in the same period.

Unfortunately, the unavailability of long time series of the observed datasets made it impossible to obtain also a quantitative integration for the selected test site.

8) AKNOWLEDGEMENTS

The authors are grateful to LiSALab Company for the GB-InSAR data processing. The TerraSAR-X data have been provided by the German Aerospace Center (DLR) under the TSX-AO (TerraSAR-X Announcement of Opportunity) project Contract #GEO0764. RADARSAT-2 data have been provided by Kongsberg Satellite Services (KSAT) through an agreement with the Norwegian Space Centre. The authors also appreciate the help from staff of the Norwegian Geotechnical Institute, which contributed to this research production: especially, they would like to thank Bjorn Kalsnes, Vidar Kveldsvik and Jose Cepeda for their support. The authors are also grateful to the NVE (Norwegian Water Resources and Energy Directorate) staff, especially they would like to thank Lars Harald Blikra, for supporting this research.

9) REFERENCES

Berardino, P.; Fornaro, G.; Lanari, R.; Sansosti E. A new algorithm for surface deformation monitoring based on small baseline differential SAR interferograms. *IEEE Trans. Geosci. Remote Sens.* **2002**, *40*, 2375–2383.

Blikra, L.H.; Braathen, A.; Derron, M.H.; Eiken, T.; Kveldsvik, V.; Groneng, G.; Dalsegg, E.; Elvebakk, H.; Roth, M. The Akerneset slope failure—A potential catastrophic rockslide in western Norway? *Abstr. Proc. Geol. Soc. Nor.* **2005**, *1*, 15–16.

Eidsvik, U.M.; Medina-Cetina, Z.; Kveldsvik, V.; Glimsdal, S.; Harbitz, C.B.; Sandersen, F. Risk assessment of a tsunamigenic rockslide at Åknes. *Nat. Hazards*, **2011**, *56*, 529–545.

Kristensen, L.; Rivolta, C.; Dehls, J.; Blikra L.H. GB-InSAR measurement at the Åknes rockslide, Norway. In Proceedings of the International Conference Vajont 1963–2013. Thoughts and Analyses after 50 years since the Catastrophic Landslide, Padua, Italy, 8–10 October 2013.

Lauknes, T.R.; Zebker, H.A.; Larsen, L. InSAR deformation time series using an L1-Norm small-baseline approach. *IEEE Trans. Geosci. Remote Sens.* **2011**, *49*, 536–546.

Lava emplacements at Shiveluch volcano (Kamchatka) from June 2011 to September 2014 observed by TanDEM-X SAR-Interferometry

A. Heck[1] (alexandra.heck@student.kit.edu), J. Kubanek[2] (julia.kubanek@kit.edu), M. Westerhaus[2], E. Gottschämmer[1], B. Heck[2], and F. Wenzel[1]

1 Geophysical Institute (GPI), Department of Physics

2 Geodetic Institute (GIK), Department of Civil Engineering, Geo- and Environmental Sciences

Outstanding Student Poster & PICO Contest

Karlsruhe Institute of Technology

Geophysical Institute KIT-Dept. of Physics

GIK

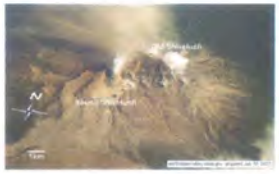

Figure 1: *Photograph of Shiveluch volcano, taken by the Expedition 15 Crew of the International Space Station.*

Introduction

As part of the Ring of Fire, Shiveluch volcano is one of the largest and most active volcanoes on Kamchatka Peninsula (Fig. 1). Since the last Plinian eruption in 1964, the activity of Shiveluch is characterized by alternating periods of dome growth, fumarolic activity and explosive eruptions. The recent active phase began in 1999 and continues until today.

As opposed to optical techniques, Synthetic Aperture Radar (SAR) is not much affected by the special conditions at active volcanoes such as volcanic plumes or poor weather conditions. However, conventional repeat-pass SAR-Interferometry (InSAR) usually fails due to strong changes at the surface between image acquisitions.

A new approach is provided by the bistatic radar data acquired by the TanDEM-X satellite mission. This mission is composed of two similar satellites, TerraSAR-X and TanDEM-X, flying in a close helix formation (Fig. 2). Since the SAR images are acquired simultaneously and the radar signals penetrate clouds and partially vegetation and loose snow, disadvantages of optical techniques and conventional InSAR can be avoided. Furthermore, the simultaneous acquisition enables the generation of DEMs.

The digital elevation model (DEM) differencing approach based on TanDEM-X bistatic data developed by Kubanek et al. (2015a and 2015b) is applied here to study topographic changes at Shiveluch volcano between June 2011 and September 2014.

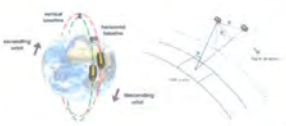

Figure 2: *Acquisition geometry of the TanDEM-X mission. For the present test site, Shiveluch and its surroundings, the incidence angle θ amounts to about 33 degrees for ascending data and for descending data it amounts to 45 degrees. Since one objective of the TanDEM-X mission is to improve the DEM accuracy by using SAR data acquired with different acquisition geometries, the distance between the two satellites, the spatial baseline B, changes over time (Fig. 4). The satellites look to the right in both orbits and operate on an average wavelength of 3.1 cm (based on Krieger et al., 2007).*

Processing

The basic idea is to calculate DEMs at different times during volcanic activity and to determine the volumetric changes by DEM differencing.

The processing was implemented with the Delft Object-oriented Radar Interferometric Software (DORIS), modified in order to process bistatic data (Fig. 3). 24 DEMs from ascending data and 18 DEMs from descending data with effective baselines between 13 m and 223 m were used (Fig. 4).

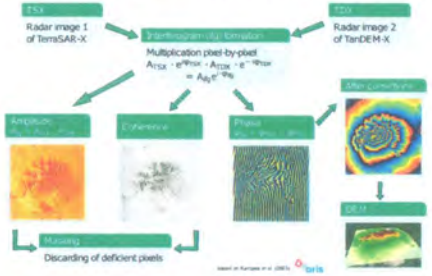

Figure 3: *Calculation of DEMs using SAR-Interferometry.*

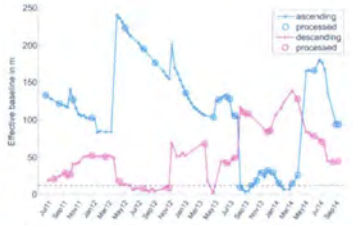

Figure 4: *Effective baselines ($B_\perp/2$, Fig. 2) of available bistatic data between June 2011 and September 2014 for the Shiveluch area. The dashed line marks an effective baseline of 12 m. Elevation models calculated with data acquired with a baseline smaller than this threshold were too noisy and could not be used for further analyses.*

Results

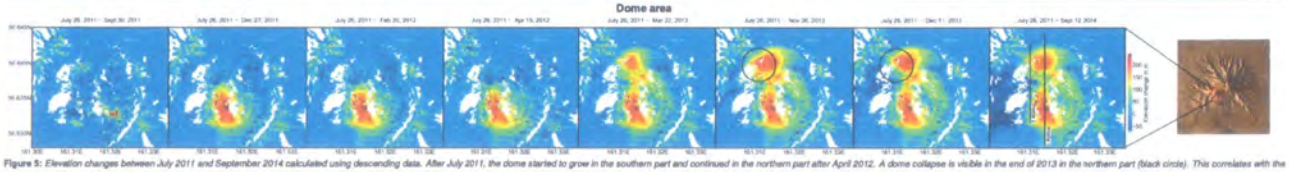

Figure 5: *Elevation changes between July 2011 and September 2014 calculated using descending data. After July 2011, the dome started to grow in the southern part and continued in the northern part after April 2012. A dome collapse is visible in the end of 2013 in the northern part (black circle). This correlates with the development of the south-western pyroclastic flow (cf. Fig 6), followed by another period of dome growth. The white areas are masked pixels with low coherence or low amplitude.*

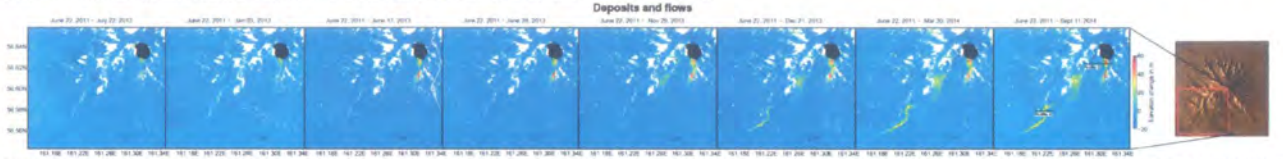

Figure 6: *Elevation changes between June 2011 and September 2014 calculated using descending data. After June 2011, a flow started to develop south of the lava dome area. A pyroclastic flow established in 2013 to the south-west, with rising volume increase after the dome collapse in the end of 2013 (cf. Fig 5). Since the dome area is analyzed with descending data, the dome area is masked out in black.*

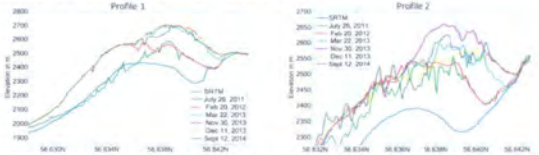

Figure 7: *Cross sections of profile 1 and 2 (see Fig. 5). In addition, the elevation data of the Shuttle Radar Topography Mission (SRTM) from February 2000 is plotted.*

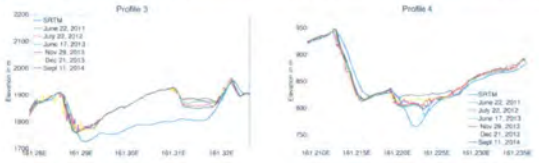

Figure 8: *Cross sections of profile 3 and 4 (see Fig. 6). In addition, the elevation data of the SRTM from February 2000 is plotted.*

The development of the lava dome and the flows is shown in Figs. 5 and 6. The DEMs have a spatial resolution of about 6 m and a vertical accuracy of about 3 m.

The cross sections of the DEMs in Fig. 7 illustrate the shape as well as the temporal development of the lava dome. The cross sections of the DEMs in Fig. 8 indicate that the juvenile material deposits primarily in depressions.

In total, the volume of the lava dome increased by 94.4 $\cdot 10^6$ m^3, the pyroclastic flow and deposits to the south-west reached a volume of 75.0 $\cdot 10^6$ m^3 and the volume of the flow in the southern part amounted to 24.1 $\cdot 10^6$ m^3 (Fig. 9). The extrusion rate reached its maximum in January 2014 with 2.4 $\cdot 10^6$ m^3/day (Fig. 10).

References

Kampes et al. (2003). *Radar Interferometry with Public Domain Tools.* In: Proceedings of FRINGE 2003, December 1-5, Frascati, Italy, 2003.

Krieger et al. (2007). *TanDEM-X: A Satellite Formation for High-Resolution SAR Interferometry.* In: IEEE Transactions on Geoscience and Remote Sensing, vol. 45, no. 11, pp. 3317-3341.

Kubanek et al. (2015a). *Volumetric change quantification of the 2012 Maroyl eruption using TanDEM-X InSAR.* In: Remote Sensing Environment, vol. 164, pp. 16-25.

Kubanek et al. (2015b). *Lava flow mapping and volume calculations for the 2012-2013 Tolbachik, Kamchatka, fissure eruption using bistatic TanDEM-X InSAR.* In: Bulletin of Volcanology 77:106.

Figure 9: *Volumetric changes of the lava dome and the deposits.*

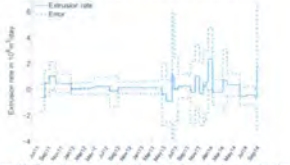

Figure 10: *Extrusion rates calculated from the volumetric changes of the lava dome and the deposits.*

NEW DEVELOPMENTS IN AMBIENT NOISE ANALYSIS FOR THE CHARACTERIZATION OF DYNAMIC RESPONSE OF SLOPES TO SEISMIC SHAKING

V. Del Gaudio[1], J. Wasowski[2]

[1] Dipartimento di Scienze della Terra e Geoambientali, Università degli Studi di Bari "Aldo Moro", Campus, via E.Orabona 4, 70125 Bari, Italy. e-mail: vincenzo.delgaudio'@'uniba.it
[2] Consiglio Nazionale delle Ricerche, Istituto di Ricerca per la Protezione Idrogeologica, Bari, Italy, e-mail: j.wasowski@ba.irpi.cnr.it

SUMMARY

Site dynamic response to seismic shaking has influence on slope failure occurrence during earthquakes. However, we don't have sufficient accelerometer data to characterize seismic response of landslide prone slopes. The analysis of ambient noise offers a good investigative alternative. Previous studies have shown that the dynamic response of slopes affected by landslides is rather complex, being characterized by multiple resonance peaks with directional variability, thus, the use of standard analysis techniques (e.g., the Nakamura method) can encounter difficulties in providing reliable information. We have recently proposed a new approach to exploit the potential of information content of Rayleigh waves present in ambient noise with regard to the identification of frequency and orientation of directional resonance. By exploiting ground motion ellipticity, this approach can also provide information on vertical distribution of S-wave velocity, which controls site amplification factors. The method, based on the identification of Rayleigh wave packets from instantaneous polarization properties of ambient noise, was first tested using synthetic signals. Then it was used to re-process and re-interpret the ambient noise data acquired on landslide prone slopes around Caramanico Terme (central Italy), at sites monitored also with accelerometer stations. The comparison of ambient noise analysis results and the accelerometer data reveals the new method can be profitably used to characterize slope dynamic response.

1) ANALYSIS METHODOLOGY

The new method of ambient noise analysis identifies Rayleigh wave packets within noise recordings using a technique of instantaneous polarization analysis to recognize Rayleigh wave typical elliptical particle motion on a vertical plane, with ellipse axes directed in horizontal and vertical directions.

To investigate polarization direction and ellipticity (i.e., the ratio H/V between horizontal and vertical ground motion amplitude) as function of wave frequency, analysis is applied to signal derived passing 3-component noise recording through narrow-band filters with different central frequency ν_c.

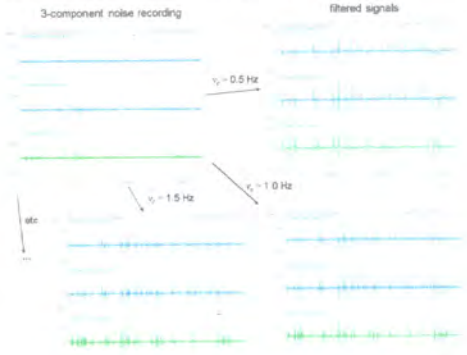

The filtered ground motion vector $\overrightarrow{u_{\nu_c}(t)}$ is analytically transformed through the equation

$$\overrightarrow{u_{\nu_c}}(t) = \overrightarrow{u_c}(t) + j\overrightarrow{\tilde{u}_c}(t) = \overrightarrow{A}(t)e^{j\theta(t)}$$

where $\overrightarrow{\tilde{u}_c}(t)$ = Hilbert transform of $\overrightarrow{u_c}(t)$, j = imaginary unit.

On the basis of this transformation, ground motion can be represented as the real part of a complex vector, which in the real space describes a time-variant elliptical trajectory. The vectors of the major and minor semi-axes of the ellipses at each instant are calculated through the formulae of Morozov and Smithson (1996). Rayleigh wave packets are recognized when a minimum number *nmin* of consecutive recording samples define elliptical trajectories whose axes lie on sub-vertical planes and deviate from horizontal/vertical direction by less than a minimum threshold *dipp*.

2) TESTS ON SYNTHETIC SIGNALS

The method capacity of determining Rayleigh wave polarization direction and ellipticity was first tested on synthetic signals simulating ambient noise, including Rayleigh and Love wave packets occasionally emerging from an incoherent Gaussian noise due to the overlapping of different types of ground vibrations. To distinguish Rayleigh from Love waves, the closeness to linear polarization of Love waves was measured through the parameter named "rectilinearity", proposed by Schimmel & Gallart (2004):

$$rl = 1 - \frac{|\vec{b}(t)|}{|\vec{a}(t)|}$$

where $\vec{a}(t)$ and $\vec{b}(t)$ are the vectors defining the instantaneous orientation and amplitude of the major and the minor semi-axis, respectively, of the elliptical particle motion. This parameter assume values between 0 (circular polarization) and 1 (linear polarization), thus a threshold *rlim* close to 1 was defined to distinguish elliptical Rayleigh waves from linear Love waves.

Test on synthetic signals characterized by different signal-to-noise ratio *snr* (i.e., the ratio between amplitude root mean square of Rayleigh waves and incoherent signals) were aimed at defining optimal choices for the threshold parameters *dipp*, *rlim* and *nmin*, allowing to recover, from instantaneous polarization analysis, Rayleigh wave characteristics with a minimum error.

Simulating conditions of directional resonance where Rayleigh waves are polarized according to a site specific preferential direction, this directivity was always correctly identified. Histograms below show the distribution among 10° azimuth interval classes of polarization directions of Rayleigh-type wave packets estimated from synthetic signals where Rayleigh waves with polarization azimuth of 37° were mixed with variably polarized incoherent signals. Even when incoherent noise has amplitudes comparable to those of Rayleigh waves (*snr* = 1) a clear maximum is observed for the azimuth class including the correct azimuth value.

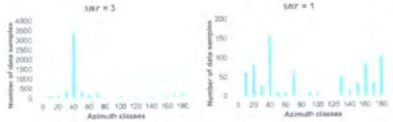

Rayleigh wave ellipticity was estimated from mean values HVIP of instantaneous ratios between maximum amplitude H_{max} of ground motion horizontal component, obtained from the analytic transformation of the E-W and N-S components only, and the amplitude V of the vertical component, obtained from this single component analytic transformation:

$$HVIP = \frac{H_{max}}{V}$$

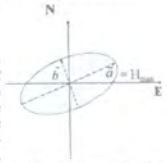

Tests showed that HVIP allows us to recognize the presence of a peak value of Rayleigh wave ellipticity around the frequency corresponding to the actual site resonance frequency. The estimate of the H/V peak value is excellent if the signal-to-noise ratios is not too low (*snr* ≥ 3), but is still quite good even for *snr* = 1, and always better than that obtained with the standard Nakamura (1989) technique, based on the calculation of mean ratios between spectral amplitude of horizontal and vertical component of noise recordings (HVNR curve in figures below).

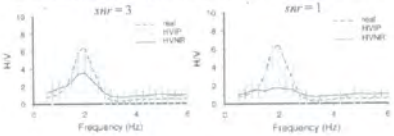

3) REAL SIGNAL TEST SITE

Tests of the new analysis methodology were carried out on ambient noise recordings acquired in 2007 at sites of accelerometer stations on landslide prone slopes in the area of Caramanico Terme and previously analysed with the Nakamura technique.

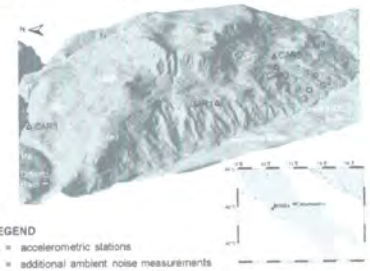

LEGEND

△ = accelerometric stations
○ = additional ambient noise measurements
Lm = limestones (Miocene)
Me = sandy-silt deposits with carbonate breccia (Messinian)
Mp = marly mudstones (Early Pliocene)
Bq = carbonate megabreccia caprock (Quaternary?)
Sqh= soils: colluvial, landslide and eluvial deposits, artificial ground (Holocene)

Station CAR2, located on a landslide consisting of colluvium overlying mudstone, is characterised by directivity in site response, whereas CAR5, located on the same kind of material, but 150 m away from the landslide, does not show evident preferential direction of maximum ground shaking during earthquakes (see to the right particle motion, in terms of acceleration on the horizontal plane, recorded during the 6 April, 2009, Mw 6.3 L'Aquila earthquake, located ~60 km NW of Caramanico).

The analysis of the azimuthal variation of mean spectral ratios (SR) between recordings of several events acquired by these stations, and those obtained for the same events at a reference station on a flat rocky site close to Caramanico (CAR4), showed for CAR2 a maximum directional amplification due N110°E at ~2.5 Hz, and other secondary peaks with similar orientation at different frequencies (see below). At CAR5, significant peaks were observed along transversal direction as well.

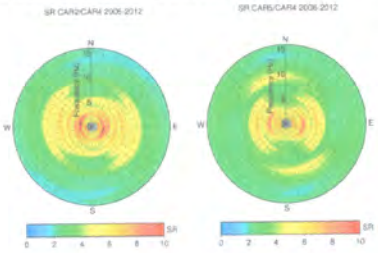

4) REAL SIGNAL TEST RESULTS

HVIP analysis was carried out on ambient noise recorded at sites CAR2 and CAR5. Instantaneous HVIP values and polarization directions were calculated for wave packets with Rayleigh-type particle motion. Results were synthesised through 3D polar histograms (see below) where, for Rayleigh-type samples with polarization direction within 10° azimuth intervals, their percentage in filtered time series is represented through the height of bars plotted as function of filtering central frequency. For each data bin, bar color represents the mean HVIP value, according to a chromatic scale.

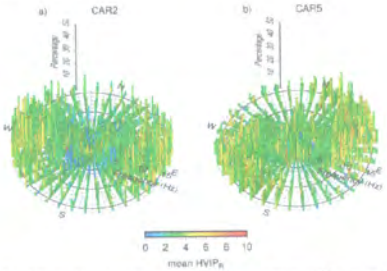

At CAR2 Rayleigh wave packets show higher percentages of data samples polarised around an approximately E-W direction, whereas at CAR5 there is lack of a persistent common preferential polarisation. Analyzing in more detail the estimate of Rayleigh wave ellipticity at CAR2, a maximum HVIP was found at 2.45 Hz for samples polarized in the azimuth interval 110°-120° and, in general, HVIP values were found larger in this direction than in an orthogonal direction, this is in good agreement with the data from seismic event recordings. On the contrary, at CAR5, there is lack of a systematic prevalence of peaks in the same direction (see below).

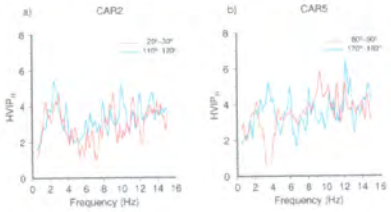

5) HVIP CURVE MODELLING

Interpreting HVIP curves, like those shown above, as an estimate of Rayleigh wave ellipticity dependence on frequency, such curves can be modelled in terms of seismic velocity vertical distribution with the support of additional constraints (e.g., from borehole stratigraphies: cf. Castellaro & Mulargia, 2009). Focusing the modelling on the reproduction of the main H/V peak, we obtained S-wave velocity models, which, in agreement with previous studies conducted using different geophysical investigation techniques (Coccia et al., 2010), confirmed that both the landslide colluvium material and the mudstone substratum are characterized at CAR2 by slower velocity than at CAR5. This suggests that slope deformations affected also the mudstone underlying the colluvium (see figure to the right).

CONCLUSIONS

Rayleigh wave packets emerging from incoherent background noise can be recognized by analyzing instantaneous polarization of ambient noise recording. Applying this analysis to noise recordings passed through narrow-band filters centered on different frequencies, one can estimate the Rayleigh wave ellipticity (i.e., the ratios H/V between the amplitudes of horizontal and vertical component of ground motion) as function of frequency. From these estimates, site resonance frequencies and directional resonance orientation can be revealed and constraints for subsurface velocity modeling can be obtained. The proposed technique relying on Rayleigh wave properties shows better performance than the classical Nakamura's method.

References

Castellaro S., Mulargia F., 2009: *VS_{30} Estimates Using Constrained H/V Measurements*. B. Seismol. Soc. Am., **99** (2A), 761–773.

Coccia S., Del Gaudio V., Venisti N., Wasowski J., 2010: *Application of Refraction Microtremor (ReMi) technique for determination of 1-D shear wave velocity in a landslide area*. J. Appl. Geophys., **71**, 71-89, doi:10.1016/j.jappgeo.2010.05.001.

Morozov I. B., Smithson S. B., 1996: *Instantaneous polarization attributes and directional filtering*. Geophysics, **61**, 872-881.

Nakamura Y., 1989: *A method for dynamic characteristics estimation of subsurface using microtremors on the ground surface*. Q. Rep. Rail. Tech. Res Inst., **30**, 25–30.

Schimmel M., Gallart J., 2004: *Degree of Polarization Filter for Frequency-Dependent Signal Enhancement Through Noise Suppression*. B. Seismol. Soc. Am., **94**, 1016–1035.